

RESEARCH ARTICLE

10.1029/2018JD028786

Special Section:

Winter INvestigation of Transport, Emissions and Reactivity (WINTER)

Key Points:

- Airborne observations show that HCl and particle chloride are dominant tropospheric Cl_y compounds in wintertime boundary layer
- Chlorine gas-particle partitioning can be modeled, assuming a small, unmeasured fraction of NaCl mass from sea salt is internally mixed
- Lower-limit equilibrium constant is derived for HCl from observations:

$$K_{eq} = 2.5 \times 10^6 \exp[5,208(1/T - 1/T_0)] \text{ mol}^2 \cdot \text{kg}^{-2} \cdot \text{atm}^{-1}$$

Correspondence to:

J. A. Thornton,
thornton@atmos.washington.edu

Citation:

Haskins, J. D., Jaeglé, L., Shah, V., Lee, B. H., Lopez-Hilfiker, F. D., Campuzano-Jost, P., et al. (2018). Wintertime gas-particle partitioning and speciation of inorganic chlorine in the lower troposphere over the Northeast United States and Coastal Ocean. *Journal of Geophysical Research: Atmospheres*, 123, 12,897–12,916. <https://doi.org/10.1029/2018JD028786>

Received 6 APR 2018

Accepted 12 OCT 2018

Accepted article online 24 OCT 2018

Published online 19 NOV 2018

Wintertime Gas-Particle Partitioning and Speciation of Inorganic Chlorine in the Lower Troposphere Over the Northeast United States and Coastal Ocean

Jessica D. Haskins¹ , Lyatt Jaeglé¹ , Viral Shah¹ , Ben H. Lee¹ , Felipe D. Lopez-Hilfiker^{1,2}, Pedro Campuzano-Jost³ , Jason C. Schroder³ , Douglas A. Day³, Hongyu Guo⁴, Amy P. Sullivan⁵, Rodney Weber⁴ , Jack Dibb⁶ , Teresa Campos⁷, Jose L. Jimenez³ , Steven S. Brown⁸ , and Joel A. Thornton¹ 

¹Department of Atmospheric Sciences, University of Washington, Seattle, WA, USA, ²Now at Laboratory of Atmospheric Chemistry, Paul Scherrer Institute, Villigen, Switzerland, ³Department of Chemistry and Cooperative Institute for Research in Environmental Sciences, University of Colorado Boulder, Boulder, CO, USA, ⁴School of Earth and Atmospheric Sciences, Georgia Institute of Technology, Atlanta, GA, USA, ⁵Department of Atmospheric Science, Colorado State University, Fort Collins, CO, USA, ⁶Institute for the Study of Earth, Oceans, and Space, University of New Hampshire, Durham, NH, USA, ⁷National Center for Atmospheric Research, Boulder, CO, USA, ⁸Chemical Sciences Division, NOAA Earth System Research Laboratory, Boulder, CO, USA

Abstract The formation of photolabile chlorine reservoirs depend on how much chloride is available in the particle to react, which requires the chlorine partitioning to the particle in the troposphere to be well understood. However, limited measurements of gas and particle composition necessary to constrain this chemistry exist. We present measurements from the Wintertime Investigation of Transport, Emissions, and Reactivity (WINTER) aircraft campaign that show inorganic tropospheric chlorine compounds (Cl_y) measured in the lower troposphere are dominated by HCl and PM₄ particulate chloride (pCl⁻), with contributions from trace chlorine species like nitryl chloride (ClNO₂), hypochlorous acid (HOCl), and molecular chlorine (Cl₂). We observed elevated Cl_y mixing ratios over the ocean (540–625 pptv) compared to over land (178–225 pptv). Observations show 0–20% (0–0.2 μg/m³) of measured chlorine partitions into particles with a diameter less than 1 μm under typical WINTER conditions. The thermodynamic model, ISORROPIA II, overpredicts submicron pCl⁻ by a factor of 2 but is brought into agreement, assuming a small fraction of unmeasured, refractory sea salt <0.1 μg/m³ exists. The model-measurement disagreement could also be caused by an effective equilibrium constant for HCl that is too large. We derive a lower-limit equilibrium function ($K_{eq} = 2.5 \times 10^6 \exp[5,208(1/T - 1/T_0)] \text{ mol}^2 \cdot \text{kg}^{-2} \cdot \text{atm}^{-1}$) that lowers the model value's temperature dependency. This work provides constraints on Cl_y in the troposphere, addresses the sensitivity of chlorine partitioning to minor changes in environmental variables, and highlights the remaining questions interfering with our ability to correctly model pCl⁻ concentrations.

1. Introduction

Multiphase photochemical cycling of tropospheric inorganic chlorine gases (Cl_y = HCl + ClNO₂ + HOCl + 2Cl₂) has been shown to have significant air quality impacts. These impacts result from the high reactivity of atomic chlorine and chlorine oxide radicals toward inorganic and organic compounds in the atmosphere (Riedel et al., 2014; Sherwen et al., 2016). Such reactions influence the abundance and partitioning of odd hydrogen (HO_x = OH + HO₂) and nitrogen oxide (NO_x = NO + NO₂) radicals, which both regulate ozone (O₃) concentrations and predominantly control the overall oxidative capacity of the atmosphere. Sherwen et al. (2016) estimated that tropospheric halogen atoms, globally, could be responsible for 15–27% of the oxidation of volatile organic compounds. Several studies have suggested that the release of chlorine atoms from multiphase photochemical cycling could be the dominant early-morning oxidative agent in the winter when HO_x radicals are less abundant (Osthoff et al., 2008; Riedel et al., 2014; Thornton et al., 2010; Young et al., 2013). However, there are very few observations to constrain chlorine chemistry in the troposphere, and until 10 years ago, it was thought to be relatively unimportant to include in tropospheric chemistry models.

Throughout the troposphere, reactive chlorine compounds are expected to be primarily in the form of hydrochloric acid (HCl) and particulate chloride (pCl⁻), with minor contributions from hypochlorous acid (HOCl),

nitryl chloride (ClNO_2), and chlorine gas (Cl_2 ; Keene et al., 1999). Together, HCl and pCl^- exist in a dynamic equilibrium that depends on highly local multiphase parameters like particle pH, liquid water content, relative humidity (RH), and solute activity (a), all of which are influenced by ambient temperature, pressure, and atmospheric composition. Unlike the nitrate equilibrium partitioning, we will show that because chloride is typically a small component in submicron aerosols, its equilibrium partitioning is largely controlled by the balance of other acids in the aerosol that drive particle pH, to which the $\text{HCl}(\text{g})/\text{pCl}^-$ equilibrium responds. As nitrate (pNO_3^-) and sulfate (SO_4^{2-}) accumulate in the aerosol, particle pH is driven lower, the activity coefficients are altered, and pCl^- is ultimately displaced into the gas phase as HCl in highly acidic submicron particles. It is important to highlight that the backward reaction of this equilibrium can occur, allowing ambient HCl to replenish available pCl^- for other reactions, like the formation of photolabile reservoirs such as ClNO_2 in areas where there is no significant primary source of pCl^- . However, the thermodynamic properties that control the phase partitioning of chlorine, such as acid dissociation constants, Henry's law constant, and the associated temperature dependencies of these quantities, have an uncertainty of nearly 3 orders of magnitude (Sander, 2015).

Guo et al. (2016) has shown that the typical pH of submicron particulate matter with a diameter less than $1\ \mu\text{m}$ ($\text{PM}_{1.0}$) sampled during the Northeastern United States winter was extremely acidic with values ranging from -1 to 3 and was primarily influenced by the bulk sulfate, nitrate, and ammonium contributions, since they were present in much larger concentrations in the aerosol than pCl^- , pNa^+ , or particulate potassium (K^+), calcium (Ca^{2+}), and magnesium (Mg^{2+}). This pH range is typical of $\text{PM}_{1.0}$ aerosols within the polluted boundary layer in the United States for other seasons and locations (Guo et al., 2015, 2016, 2017).

It is important to understand the chloride partitioning to the particle phase, since the abundance of photolabile Cl^- reservoirs, such as ClNO_2 , Cl_2 , or BrCl (Behnke et al., 1997; Finlayson-Pitts et al., 1989; Roberts et al., 2009; Sarwar et al., 2014; Vogt et al., 1996), directly depends on how much chloride is available in the particle to react, as do parameterizations that attempt to dynamically predict their formation (Bertram & Thornton, 2009). Consequently, it is important to constrain the magnitude of the sources of pCl^- and HCl and their multiphase partitioning to accurately assess the scale of tropospheric reactive chlorine impacts on air quality and greenhouse gas lifetimes. There are limited simultaneous measurements of pCl^- , HCl , and aerosol and gas composition necessary to constrain this chemistry, complicating the ability to observationally verify model predictions of tropospheric chlorine activation and its environmental impacts. Here we present an analysis of observations obtained during the 2015 Wintertime Investigation of Transport, Emissions, and Reactivity (WINTER) aircraft campaign to provide constraints on tropospheric inorganic Cl_y and its submicron gas-particle partitioning.

2. Methods

2.1. Campaign and Instrumentation

The WINTER campaign took place in February and March of 2015 using the National Science Foundation/National Center for Atmospheric Research (NCAR) C-130 aircraft, with instruments measuring a rich suite of chemical compounds, including O_3 , NO_x , HCl , HOCl , Cl_2 , ClNO_2 , volatile organic compounds, dinitrogen pentoxide (N_2O_5), nitric acid (HNO_3), peroxyacyl nitrates, and aerosol composition over 13 flights over the eastern United States during both day and night above rural and highly populated areas. Flight patterns were designed to capture air masses downwind of coastal polluted regions throughout the night within the boundary layer when nitrogen and halogen coupled heterogeneous processing occurs. In this work, focus will be given to data taken using the University of Washington's high-resolution time-of-flight chemical ionization mass spectrometer, the University of Colorado's high-resolution time-of-flight aerosol mass spectrometer, Georgia Tech's particle-into-liquid sampler (PILS) and ion chromatograph (IC), and the University of New Hampshire's (UNH's) bulk aerosol filter measurements, restricted to areas that were not sampled in cloud.

2.1.1. CIMS

A high-resolution time-of-flight chemical ionization mass spectrometer (hereafter referred to as "CIMS") using iodide-adduct ionization (Lee et al., 2014; Lopez-Hilfiker et al., 2016) was used to simultaneously detect, at 2 Hz, HNO_3 , HCl , ClNO_2 , N_2O_5 , Cl_2 , HOCl , and chlorine nitrate (ClONO_2), among other trace gases. Iodide ions are produced by passing methyl iodide past a Po-210 foil and mixed with ambient air in a low-pressure (80 mbar) flow reactor to selectively cluster with target gases in ambient air. A small fraction of the

Table 1

Limits of Detection for Species Measured by the PILS, AMS, and CIMS at Two Different Sampling Periods, 10 s and 5 min (Shown in Parentheses), Used in This Study

Measured Species	PILS-IC	AMS	CIMS
	10 s (5 min)	10 s (5 min)	10 s (5 min)
Nitrate ($\mu\text{g}/\text{m}^3$)	0.21 (0.04)	0.022 (0.004)	—
Sulfate ($\mu\text{g}/\text{m}^3$)	0.26 (0.05)	0.006 (0.001)	—
Chloride ($\mu\text{g}/\text{m}^3$)	0.51 (0.09)	0.022 (0.004)	—
Ammonium ($\mu\text{g}/\text{m}^3$)	—	0.003 (0.0006)	—
HCl (pptv)	—	—	22 (4.7)
HOCl (pptv)	—	—	1.0 (0.23)
Cl ₂ (pptv)	—	—	0.1 (0.02)
CINO ₂ (pptv)	—	—	0.1 (0.03)

Note. PILS = particle-into-liquid sampler; IC = ion chromatograph; AMS = aerosol mass spectrometer; CIMS = chemical ionization mass spectrometer.

reaction mixture is continuously sampled into the mass spectrometer where ions are ultimately separated by their time of flight; used to determine their mass to charge, m/Q , to within 15 ppmv; and counted using a microchannel plate detector.

Calibrations for all gas-phase species used in this work are performed through a variety of methods described in more detail in Lee et al. (2014), with a methodology of our calibration methods and uncertainty estimates for compounds measured with the CIMS during the WINTER campaign found in Lee et al. (2018). The WINTER mean 10-s detection limits (DLs) are 22 pptv for HCl, 2.2 pptv for HNO₃, 1 pptv for HOCl, and 0.1 pptv for Cl₂, CINO₂, and N₂O₅. These DLs are a function of both sensitivity and background level, neither of which is a constant, as they can vary with ion molecule reactor (IMR) water vapor pressure and polluted air parcels, respectively. The background noise for chlorine-containing compounds are typically lower than those composed only of carbon, oxygen, and hydrogen atoms since chlorine-containing compounds have large negative mass defects. Therefore,

the DLs of chlorine-containing compounds are mainly a function of their sensitivity to iodide-adduct ionization and noise detector (Lee et al., 2018). The estimated uncertainty for the reported data is $\pm 30\%$ for HCl, CINO₂, Cl₂, HOCl, N₂O₅, and HNO₃, for which a direct calibration was performed, and the uncertainty represents a conservative estimate of the variability in measured sensitivity. For other species, we rely on calculations of sensitivity, and the uncertainty (typically $\pm 50\%$) stems from the scatter about the relationship between calculated and measured sensitivities (Lee et al., 2018). A calibration for CINO₃ is not yet available, and thus, we neglect it in this analysis. For the following analysis, values from the CIMS reported below the DL are set to values equal to one-half DL.

2.1.2. Particle Measurements

Nonrefractory ions in particles with a wet diameter less than 1 μm were sampled with a high-resolution time-of-flight aerosol mass spectrometer (hereafter referred to as an “AMS”) at 1 Hz in total aerosol mass mode. The general operation of the AMS has been described in detail previously (Canagaratna et al., 2007; DeCarlo et al., 2006; Jayne et al., 2000; Kimmel et al., 2011), and specifics about the operation of the AMS during the WINTER campaign are described in Guo et al. (2016) and Schroder et al. (2018). Relative ionization efficiencies for pSO_4^{2-} , pNH_4^+ , pNO_3^- , and pCl^- were determined by multiple in-field calibrations. The estimated overall accuracy for AMS detection of inorganic species is estimated at 35% for aircraft operation (Bahreini et al., 2008). Typical DLs during WINTER were 137 (57) ng/sm^3 for pSO_4^{2-} , 12 (5) ng/sm^3 for pNH_4^+ , 69 (30) ng/sm^3 for pNO_3^- , 77 (32) ng/sm^3 for pCl^- , and 474 (194) ng/sm^3 for organic aerosol for a 1-s (1-min) sampling interval (sm^3 refers to cubic meters at standard temperature and pressure; Schroeder et al., 2018). Refractory species, such as salts like NaCl, NaNO₃, and Na₂SO₄, are inefficiently detected by the AMS (Hayes et al., 2013), meaning that the reported submicron pCl^- measurement does not contain significant contributions from sea salt, but rather species like NH₄Cl and KCl.

To account for missing refractory components of the aerosol, including NaCl, water-soluble ions in particles with a wet diameter less than 1 μm were sampled with a PILS that was coupled with two ICs. Due to lower sensitivity for the cation separation method used compared with the anion method employed during the campaign, the cation IC was determined to have DLs too high to confidently report measurements of pNH_4^+ and pNa^+ (comprehensive operational discussion provided in Guo et al., 2016). Only data from the anion IC were available for the campaign (i.e., measurements of pCl^- , pNO_3^- , and pSO_4^{2-}). Because of this, the AMS provided the only submicron measurement of pNH_4^+ , which is a critical buffering cation in a deliquesced aerosol in determining aerosol pH in the polluted marine boundary layer. Furthermore, it was found that only 19% ($n = 106$) of the pCl^- measurements were above the 0.09- $\mu\text{g}/\text{m}^3$ DL of the PILS-IC on a 5-min time period (Table 1). Therefore, in explicitly calculating the equilibrium partitioning of reactive chlorine in a Cl^- - Na^+ - SO_4^{2-} - NH_4^+ - NO_3^- -water inorganic aerosol system, the AMS data were found to be most useful for PM₁ particles, though we use the PILS measurements, when available, as a constraint on the upper limit for PM₁ pCl^- . We thus evaluate whether nonrefractory pCl^- is sufficient to explain HCl/ pCl^- partitioning and, if not, how much of an error using it may cause.

A PILS fraction collector was also present, providing offline measurements of $p\text{Na}^+$ with a DL of $0.001 \mu\text{g}/\text{m}^3$ in PM_{10} that used a different model cation IC. It also measured $p\text{Cl}^-$, but like the PILS-IC, the DL was $0.1 \mu\text{g}/\text{m}^3$, which was higher than most points of observation. As such, we did not use these measurements in assessing the chlorine partitioning but use the PILS fraction collector measurements when available, as a constraint for PM_{10} $p\text{Na}^+$. The PILS with a fraction collector setup was similar to the PILS-IC, except with a higher liquid flow rate of $0.72 \text{ ml}/\text{min}$ over the impactor to allow collection of the PILS liquid sample into 2-ml polypropylene fraction collector vials, which is described in Sorooshian et al. (2006). A vial was collected every 2 min continuously during each flight. The vials were analyzed for carbohydrates following the method of Sullivan et al. (2014).

In addition, a filter sampling system was used to collect particles with a wet aerodynamic diameter less than $4.1 \mu\text{m}$ (PM_{4}) with a 50% passing efficiency (McNaughton et al., 2007), which were subsequently analyzed for water-soluble ions by IC, as described in Dibb et al. (1999, 2000). The filter sampling time was on average 5 min but varied across each flight depending on the flight path being flown. This aerosol composition measurement technique will capture contributions from sea-salt aerosols with diameters approximately less than $4.1 \mu\text{m}$, larger than the two PM_{10} composition measurements. However, it is important to note that considerable sea-salt mass potentially lies in larger particles that would not be collected by this measurement technique. Therefore, the measurements of particle chloride taken during WINTER reflect a lower limit of the total chloride mass present in the atmosphere.

Particle size distributions in cloud-free air were measured at 10 Hz with a Particle Measuring System Passive Cavity Aerosol Spectrometer Probe (PCASP/Signal Processing Package-200; Strapp et al., 1992; Snider & Petters, 2008) for particles with a wet diameter between 0.1 and $3 \mu\text{m}$. Uncertainty in the airborne aerosol volume concentration derived from particle sizes measured by the PCASP has previously been estimated at $\pm 20\%$ (Snider & Petters, 2008).

2.2. ISORROPIA II: Thermodynamic Equilibrium Partitioning Model

2.2.1. Model Description

We use the ISORROPIA II (Fountoukis & Nenes, 2007) thermodynamic model to determine the composition of the Cl^- - Na^+ - SO_4^{2-} - NH_4^+ - NO_3^- -water inorganic aerosol system during the 2015 WINTER aircraft campaign. In our calculations, we provide ISORROPIA II with total (gas + PM_{10}) composition and ambient conditions, and the model partitions species into either the gas or the particle in thermodynamic equilibrium with the system (i.e., run in forward mode). For example, total chloride inputs to the model are the sum of the measured gas-phase HCl from the University of Washington's CIMS and a measurement of the $p\text{Cl}^-$ from one of the submicron particle composition instruments, and ISORROPIA II calculated the equilibrium concentrations of HCl and submicron $p\text{Cl}^-$. Because particle- and gas-phase measurements were made separately during the WINTER campaign, it is then possible to verify whether the model has correctly partitioned those compounds. In addition, we calculate particle pH and liquid water content following Guo et al. (2015, 2016, 2017). All concentrations reported here for particle-phase species are at ambient conditions.

2.2.2. ISORROPIA II Simulations

In all ISORROPIA II simulations, we assume equilibrium of internally mixed, chlorine-containing, submicron aerosols with the gas phase. Although most sea-salt mass is contained in larger particles that are externally mixed, and that coexist with the accumulation mode (Keene et al., 1999), these externally mixed particles have a significantly longer equilibration time with the gas phase. Additionally, most size-resolved estimates suggest the pH of these larger particles is higher than those in the submicron due to a larger buffering capacity of the nonvolatile cations that dominate that mode (Fang et al., 2017; Zaveri et al., 2008) such that it may not be thermodynamically favorable for these particles to displace chloride into the gas phase as HCl (requires $\text{pH} < \sim 3$). The assumption of internal mixing is based on coagulation cloud processing and nitrate partitioning. We effectively assume that since HNO_3 is in equilibrium with particles that do not contain NaCl, such as those containing NH_4^+ - SO_4^{2-} , over time, NO_3^- will migrate to particles containing NaCl since NaNO_3 is a more stable form of nitrate than NH_4NO_3 , resulting in a mixed aerosol.

During the WINTER campaign, NH_3 was measured using a heated inlet line with a long residence time leading partial conversion of particulate ammonium into gas-phase NH_3 prior to detection. Therefore, following Guo et al. (2016), we chose not to use these NH_3 data. Guo et al. (2016) showed that including the WINTER NH_3 data in their ISORROPIA II analysis caused the resulting particulate NO_3^- to be overpredicted by 65%

Table 2
ISORROPIA II Inputs Used in This Study of 2015 WINTER Campaign Chlorine Partitioning

ISORROPIA inputs	Base	Iterated NaCl
Total nitrate	CIMS HNO ₃ + AMS NO ₃ ⁻	CIMS HNO ₃ + AMS NO ₃ ⁻
Total sulfate	AMS SO ₄ ²⁻	AMS SO ₄ ²⁻
Total ammonium	AMS NH ₄ ⁺ + iterated NH ₃	AMS NH ₄ ⁺ + iterated NH ₃
Total chloride	CIMS HCl + AMS Cl ⁻	CIMS HCl + iterated Cl ⁻
Sodium	0	Iterated Na ⁺

Note. WINTER = Wintertime Investigation of Transport, Emissions, and Reactivity; AMS = aerosol mass spectrometer; CIMS = chemical ionization mass spectrometer.

compared to measurements from the AMS and PILS instruments during the WINTER campaign. To address this error in nitrate partitioning, Guo et al. (2016) iterated ISORROPIA II using the predicted NH₃ concentrations to calculate total ammonia ($T\text{NH}_3 = \text{NH}_3 + \text{NH}_4^+$) as input for the next iteration, until the ISORROPIA II NH₄⁺ predictions converged with the measurements of NH₄⁺. They showed that the WINTER mean NH₃ concentrations were 0.10 μg/m³ (10th percentile = 0.0 μg/m³ and 90th percentile = 0.25 μg/m³), and most of the ammonia (91% ± 22%) partitions to the particle phase. The predicted nitrate partitioning was in much better agreement with the measurements when using the iterated solution or when neglecting the NH₃ data entirely. Furthermore, particle pH changed by only approximately 3% (slope = 0.97 and R² = 0.81), with a pH systematically ~0.2 pH units higher for the iterated solution compared to not

including NH₃ data. As Guo et al. (2017) showed, particle pH is not highly sensitive to NH₃, requiring 10 times change in NH₃ for a unit change in pH.

Following Guo et al. (2016), we iterate the thermodynamic model, adjusting $T\text{NH}_3$, until the pNH₄⁺ prediction converges with observations, to be as conservative as possible with regard to particle acidity, considering the more reliable measurements of gas and particle composition that drives particle acidity made during the WINTER campaign. In the mean, we measure an estimated 91% of all the submicron $T\text{NH}_3$ with the AMS and PILS, and our resulting estimation for gas-phase NH₃ is small enough that it does not impact the pH significantly enough to change the chlorine-partitioning results we present outside the uncertainty ranges of the measurements.

For our simulations, ISORROPIA II is run in “metastable” mode, which suppresses any solid precipitates from forming. Following Guo et al. (2016), we exclude data with RH < 20%, since under these conditions, aerosols are less likely to be in a completely liquid state, or within the boundary layer (Ansari & Pandis, 2000; Fountoukis & Nenes, 2007; Malm & Day, 2001), and the modeled activity coefficients associated with such highly concentrated solutions are very uncertain (Fountoukis et al., 2009). Owing to the exponential growth in particle liquid water with RH, data with RH > 95% are assumed to have an RH = 95% (only 4% of data). Neglecting these two effects in ISORROPIA II analysis has been shown to affect the model-predicted pH (Guo et al., 2015, 2016; Malm & Day, 2001) and, therefore, the partitioning of HNO₃ and HCl to the gas phase. We subsequently analyze the potential effects of uncertainty in phase state and activity coefficients even within this RH range.

We run ISORROPIA II using 10-s averages of WINTER observations of total chloride ($T\text{Cl} = \text{HCl} + \text{pCl}^-$), total nitrate ($T\text{NO}_3 = \text{HNO}_3 + \text{pNO}_3^-$), pSO_4^{2-} , pNH_4^+ , and estimated NH₃, as well as temperature, pressure, and RH. In a first simulation (“Base” simulation in Table 2), we use pCl^- from the AMS ($D_p < 1 \mu\text{m}$) and HCl from the CIMS to calculate $T\text{Cl}$. As noted in section 2.1.2, the AMS only detects nonrefractory pCl^- (i.e., NH₄Cl, HCl (aq)), not NaCl, which is also likely to be present in PM₁ aerosol. We will show that this simulation likely underestimates the amount of $T\text{Cl}$. Guo et al. (2016) performed an ISORROPIA II analysis using both the PILS fraction collector data and the AMS data as input for the particle concentrations and showed that both gave similar results for predicted fine-particle pH. In this analysis, we use the AMS particle composition data as ISORROPIA II input since the pCl^- measurements were well above their DLs, while the PILS-IC and PILS fraction collector pCl^- measurements were not.

In a second ISORROPIA II simulation (“Iterated NaCl”), we estimate the potential influence of fine-mode sea salt (pNa^+ and pCl^-) not detected by the AMS by simultaneously iterating the thermodynamic calculation with changing amounts of $T\text{NH}_3$, and $T\text{Cl}$ in equal molar amounts with pNa^+ , until the predicted HCl and pNH_4^+ concentrations simultaneously converge with the observations within their DLs. Table 2 summarizes the differences in these ISORROPIA II simulations. Any chloride added was assumed to be in the form of NaCl, so equal molar amounts of pNa^+ and $T\text{Cl}$ were added concurrently, constrained by the gas-phase HCl measurements (i.e., how much pCl^- was added until predicted HCl matched the observed HCl; the same amount of pNa^+ was added). The iterated $T\text{Cl}$ concentrations were required to be equal to or greater than the sum of the AMS pCl^- and CIMS HCl measurements,

simulating only addition of total chloride. Convergence was required within 30 iterations with a tolerance of either $\pm 10\%$ of the input measurement or $\pm 0.018 \mu\text{g}/\text{m}^3_{\text{amb}}$ of pNH_4^+ and ± 15 pptv of HCl, whichever was largest.

In this simulation, chlorine-partitioning agreement is forced to be within the DLs of the HCl observation, a tight constraint to ensure the most accurate predictions of $^{\text{T}}\text{Cl}$ allowable with this method. The estimation of NH_3 from the iteration method was done simultaneously with the estimate of additional NaCl by the iteration of $^{\text{T}}\text{Cl}$ and pNa^+ since the presence of some amount of submicron NaCl would affect particle pH and therefore the amount of NH_3 needed to match the predicted and observed pNH_4^+ partitioning. Over 85% ($n = 16,320$) of all observations passed to the model for evaluation resulted in values of NH_3 , pNa^+ , and pCl^- , for which mutual convergence was found. The median pH change from adding submicron NaCl in this simulation was +0.02 units from the base simulation because not all points needed additions of NaCl, and when they did, the addition did not significantly impact pH, and therefore did not significantly impact partitioning of nitrate, chloride, or ammonium. Furthermore, the mean change in the amount of NH_3 estimated in this simulation from the base simulation was $0.0 \mu\text{g}/\text{m}^3$. The effect on submicron particle pH from our simulations is consistent with the conclusion in Guo et al. (2016) that pNa^+ and pCl^- do not significantly perturb PM_1 pH, such that the submicron chloride partitioning is dependent upon the pH but does not determine it.

3. Results and Discussion

3.1. Measurements of Cl_y Compounds

Figure 1 and Table 3 give a summary of the observed WINTER $^{\text{T}}\text{Cl}_y$ ($^{\text{T}}\text{Cl}_y = \text{Cl}_y + \text{pCl}^-$) compounds subdivided into air masses sampled over the ocean and over land during the day and night in the bottom 1 km of the atmosphere. Day and night were defined using local time of observations with 10 a.m.–6 p.m. defined as day and the opposite as night. Only points where simultaneous measurements of all chlorine compounds (e.g., HCl, HOCl, Cl_2 , ClNO_2 , UNH pCl^- , PILS pCl^- , and AMS pCl^-) were made are included in the data presented in Figure 1 and Table 3. All concentrations shown are calculated using data from observations time averaged over the sampling period of the UNH filters, which was typically 5–7 min. Values where an individual measurement is found to be below the time-averaging adjusted DL are set to a value of half the DL (reported in Table 1) and are included. It should be noted that the WINTER campaign did not spend equal amounts of time sampling these regions, and the sample size and highly local nature of many of the gas-phase Cl_y components influences the trends shown in Figure 1 and Table 3. The percentages presented in Figure 1 are only representative of the relative abundances of the chlorine-containing compounds measured during WINTER. In line with expectations and past studies (Graedel & Keene, 1995), $^{\text{T}}\text{Cl}_y$ concentrations are elevated over the ocean with respect to those over land with the median total mixing ratio of $^{\text{T}}\text{Cl}_y$ found over the ocean at night being 625 pptv and during the day being 540 pptv. Over land the median total mixing ratio of $^{\text{T}}\text{Cl}_y$ was 225 pptv over land at night and 178 pptv during the day. In all cases, we found that the largest concentrations of measured $^{\text{T}}\text{Cl}_y$ were from HCl and $\text{PM}_4 \text{pCl}^-$. ClNO_2 , HOCl, and Cl_2 were present at lower abundances compared to HCl but can have a more significant impact on tropospheric chemistry.

Measurements obtained during the WINTER campaign represent one of the more comprehensive atmospheric HCl data sets reported to date and are well in line with prior measurements and chlorine inventories (Keene et al., 2007) both over the ocean and over land. In pristine areas of the marine boundary layer where anthropogenic contributions are minimal, chloride displacement from HNO_3 and H_2SO_4 uptake to sea spray aerosol is the largest source of lower tropospheric HCl (Keene et al., 1999). Over land, HCl can also be emitted from the combustion of coal containing chloride by power plants. The median mixing ratio of HCl observed during the WINTER campaign was 305 pptv over the ocean at night, 329 pptv over the ocean during the day, 113 pptv over land at night, and 100 pptv over land during the day. Sustained, elevated HCl concentrations were observed in the range of 1,800 pptv offshore on several flights in areas that are not likely impacted by anthropogenic emission of HCl but rather secondary production of HCl from equilibrium partitioning out of the particle. The highest concentrations of HCl ($>5,000$ pptv) were measured within freshly emitted coal-fired power plant plumes (Lee et al., 2018).

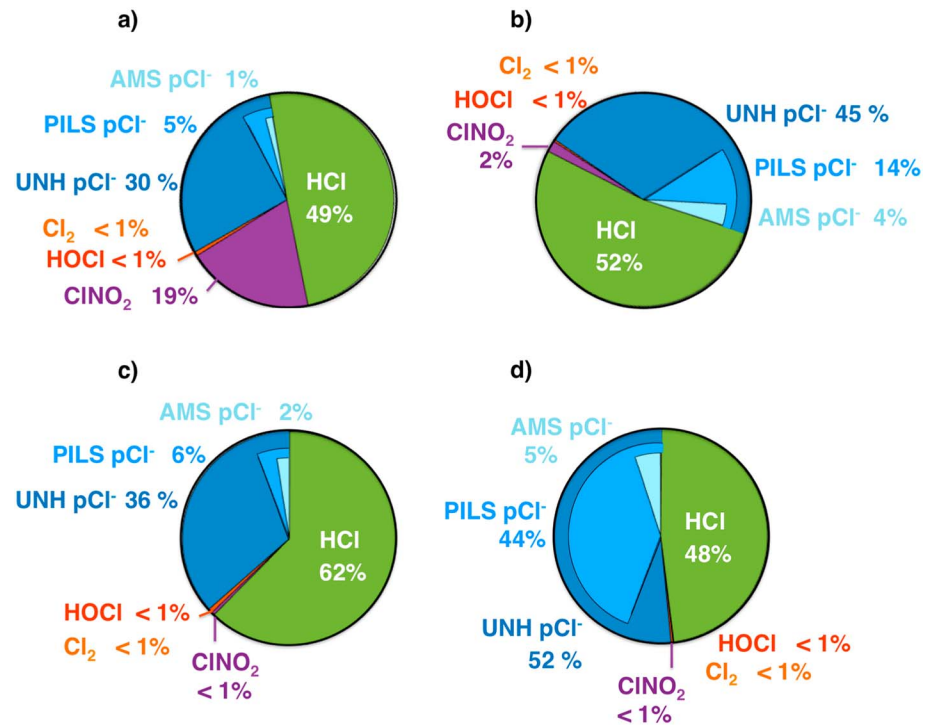


Figure 1. Median values of the various inorganic chlorine compounds measured within the boundary layer (<1 km) (a) over the ocean at night, (b) over land at night, (c) over the ocean during the day, and (d) over land during the day.

The total amount of PM₄ pCl⁻ sampled by the UNH Soluble Acidic Gases and Aerosol (SAGA) instrument is elevated over the ocean, with median concentrations of 0.2–0.5 μg/m³, compared to 0.15 μg/m³ over land within the boundary layer. The PILS provided constraints on the upper limit of PM₁ pCl⁻. However, only 21% (*n* = 106) of the PILS-IC measurements below 1-km altitude were above

Table 3
The Median, 25% Quartile (Q1), and 75% Quartile (Q3) of the Concentrations of Cl_{*i*} Measured Below 1 km in Altitude

Measured Species	Over ocean, night	Over ocean, day	Over land, night	Over land, day
No. of observations	79	11	58	47
UNH pCl ⁻	188 pptv (Q ₁ : 104, Q ₃ : 328) 0.28 μg/m ³ (Q ₁ : 0.16, Q ₃ : 0.50)	192 pptv (Q ₁ : 86, Q ₃ : 294) 0.29 μg/m ³ (Q ₁ : 0.13, Q ₃ : 0.43)	98 pptv (Q ₁ : 39, Q ₃ : 154) 0.15 μg/m ³ (Q ₁ : 0.06, Q ₃ : 0.23)	87 pptv (Q ₁ : 49, Q ₃ : 113) 0.12 μg/m ³ (Q ₁ : 0.07, Q ₃ : 0.17)
PILS pCl ⁻	—* —*	—* —*	—* —*	75 pptv (Q ₁ : 32, Q ₃ : 129) 0.10 μg/m ³ (Q ₁ : —*, Q ₃ : 0.18)
AMS pCl ⁻	8.4 pptv (Q ₁ : 5.6, Q ₃ : 11) 0.01 μg/m ³ (Q ₁ : 0.01, Q ₃ : 0.02)	13 pptv (Q ₁ : 11, Q ₃ : 22) 0.02 μg/m ³ (Q ₁ : 0.1, Q ₃ : 0.03)	8.8 pptv (Q ₁ : 7.2, Q ₃ : 12) 0.01 μg/m ³ (Q ₁ : 0.01, Q ₃ : 0.02)	11 pptv (Q ₁ : 8.3, Q ₃ : 16) 0.02 μg/m ³ (Q ₁ : 0.01, Q ₃ : 0.03)
HCl	305 pptv (Q ₁ : 199, Q ₃ : 370)	329 pptv (Q ₁ : 240, Q ₃ : 380)	113 pptv (Q ₁ : 69, Q ₃ : 202)	100 pptv (Q ₁ : 74, Q ₃ : 158)
ClNO ₂	119 pptv (Q ₁ : 24, Q ₃ : 317)	2.5 pptv (Q ₁ : 0.9, Q ₃ : 270)	3.7 pptv (Q ₁ : 0.9, Q ₃ : 8.2)	1 pptv (Q ₁ : 0.1, Q ₃ : 3)
HOCl	3.9 pptv (Q ₁ : 2.3, Q ₃ : 6.3)	3.4 pptv (Q ₁ : 2, Q ₃ : 4.6)	0.64 pptv (Q ₁ : 0.38, Q ₃ : 1.9)	0.6 pptv (Q ₁ : 0.1, Q ₃ : 1)
Cl ₂	0.60 pptv (Q ₁ : 0.28, Q ₃ : 1.6)	0.27 pptv (Q ₁ : 0.2, Q ₃ : 3)	0.1 pptv (Q ₁ : 0.08, Q ₃ : 0.21)	0.18 pptv (Q ₁ : 0.09, Q ₃ : 0.3)
Sum median mixing ratio	625 pptv	540 pptv	225 pptv	178 pptv

Note. Each observation represents an average concentration taken over the sampling period of the UNH filter measurements (5–7 min). —* indicates that Q₁, median, and Q₃ are all equal to one-half detection limit. UNH = University of New Hampshire; PILS = particle-into-liquid sampler; AMS = aerosol mass spectrometer.

the DL of $0.09 \mu\text{g}/\text{m}^3$, with resulting median mixing ratios of one-half its DL, $0.045 \mu\text{g}/\text{m}^3$, over the ocean and over land except for samples taken over land during the day where a median of $0.1 \mu\text{g}/\text{m}^3$ was detected. The lower limit on $\text{PM}_{10} \text{pCl}^-$ is provided by the AMS nonrefractory chloride measurement with a median of $0.01\text{--}0.02 \mu\text{g}/\text{m}^3$, which is well below the PILS DL. The largest concentrations of AMS $\text{PM}_{10} \text{pCl}^-$, $\sim 0.20 \mu\text{g}/\text{m}^3$, were observed downwind of New York City over the Atlantic during Research Flight 3 on the night of 7 February 2015, where most of the other Cl_y compounds were also elevated.

ClNO_2 sampled during the WINTER campaign peaks at night at over the ocean with a median mixing ratio of 119 pptv below 1 km on a 5- to 7-min averaging period. In plumes offshore, ClNO_2 reached 1,000 pptv lasting well into the early morning until nearly 10 a.m. local time. The WINTER campaign intentionally targeted areas where ClNO_2 production would be maximized over the ocean at night, and observations show large enhancements of ClNO_2 in obvious plumes on flights in the polluted offshore regions downwind of New York City but also significantly smaller concentrations in the same area on different flights, highlighting the highly local and variable nature of its production. In the median we observed <4 pptv of ClNO_2 over land, but we observed localized plumes upward of 70 pptv at night, which is enough to significantly impact the morning radical budget in the winter (Riedel et al., 2013). The WINTER observations of ClNO_2 are in generally good agreement in the overall pattern of the diurnal cycling and median boundary layer concentrations with all previous measurements of data collected in both coastal and continental regions (Bannan et al., 2015; Faxon et al., 2015; Mielke et al., 2011, 2013; Osthoff et al., 2008; Phillips et al., 2012; Riedel et al., 2012, 2013; Tham et al., 2014; Thornton et al., 2010).

We observed HOCl up to 43 pptv within 1 km over the ocean at night on a 5- to 7-min time-averaging period. However, we would expect its concentration to peak during the day (Lawler et al., 2011; Saiz-Lopez et al., 2012; Simpson et al., 2015). There was evidence of direct emissions of HOCl over land inside of targeted power plant plumes of up to 62 pptv, which quickly diluted downwind. Lawler et al. (2011) presented measurements of HOCl from a CIMS using a bromide-adduct ion at Cape Verde off the coast of Africa positioned approximately 50 m from shore from 30 May to 7 June 2009. They report distinctive diurnal trends with HOCl concentrations peaking during the day with an approximate daytime mean of 80 pptv during only the first 4 days of the campaign with notably smaller diurnal trends and absolute concentrations during the half of the campaign with an approximate daytime mean of 9 pptv. During the day, on Research Flight 13 off the coast of South Carolina, we observed sustained HOCl concentrations greater than 20 pptv, similar to those observed in the second half of the sampling period presented in Lawler et al. (2011) but notably smaller than those observed during the first half of the sampling period. The HOCl data from Research Flight 13 are not included in the data presented in Figure 1 and Table 3 because the PM_{10} measurements were not simultaneously detected on that flight. If included, the median WINTER HOCl concentration below 1 km over the ocean during the day increase from 3.9 to 5.6 pptv. However, the air masses sampled during the WINTER campaign were notably more polluted than during the relatively clean marine air sampled during the Cape Verde campaign. Additionally, both the sampling method and calibration to HOCl, NO_y , O_3 , CO, and Cl_2 concentrations were different enough during the two campaigns, to account for these differences in what is known to be highly localized photochemical cycling.

We observed Cl_2 concentrations elevated over the ocean at night, with concentrations ranging from only 0.12 to 0.6 pptv in the median over a 5- to 7-min time period, but with local concentrations up to 12 pptv in the polluted offshore region downwind of New York City. Daytime concentrations of 1–2 pptv were observed during Research Flight 13 off the shore of South Carolina, where HOCl concentrations were maximized, but other daytime ocean observations were limited. Concentrations were also elevated over land within specific power plant plumes (Lee et al., 2018). Elevated Cl_2 concentrations were spatially correlated with elevated nighttime ClNO_2 concentrations over the ocean, suggesting that coproduction via heterogeneous processes like those presented in Roberts et al. (2008) may be possibly occurring. However, these elevated plumes originated over areas where the anthropogenic release of Cl_2 may also be responsible for their elevated levels. Our Cl_2 measurements are generally in good agreement with those presented in Lawler et al. (2011) showing Cl_2 peaking at night with concentrations ranging from 10 to 20 pptv and 1 to 2 pptv during the day. Like

Lawler et al. (2011), we did not always see elevated Cl_2 levels during night, reflecting the highly variable nature of this compound in the lower troposphere.

One key question of this work is whether the displacement of chloride from sea-salt particles can explain the elevated levels of gas-phase Cl_y observed over the ocean or whether anthropogenic emission and transport of Cl_y or sources of pCl^- other than sea salt may play a larger role in determining the tropospheric halogen budget, which was last estimated in the early 1990s (Keene et al., 1999). We use the UNH observations of pNa^+ and pCl^- to calculate the absolute chloride mass displaced from a sea-salt particles, dCl^- , which is shown in Figure 2b. Previous comparisons of the pCl^- -to- pNa^+ ratio in fresh sea spray have shown it to be conserved, with a measured mass ratio of 1.78 (Junge & Werby, 1958). The dCl^- is calculated by subtracting the measured pCl^- from the maximum amount of chloride present in sea-salt particles, which is the product of the measured amount of pNa^+ , and the Cl^- -to- Na^+ mass ratio in seawater, $(\text{Cl}^-/\text{Na}^+)_{\text{seawater}} = 1.78$:

$$\text{dCl}^- = \text{pNa}^+ \left(\frac{\text{Cl}^-}{\text{Na}^+} \right)_{\text{seawater}} - \text{pCl}^-$$

Over the ocean below 1 km, 45% (202 pptv) of the median total measured gas-phase Cl_y (448 pptv) is explained by the amount displaced from PM_4 sea-salt particles. Over land, there is less total Cl_y below 1 km (116 pptv), but chloride displacement from sea salt still only explains 45% (53 pptv) of the observed Cl_y . The excess Cl_y that is unexplained by displacement from sea-salt particles ($\text{Cl}_y - \text{dCl}^-$) is shown in Figure 2c. Over the ocean, 280 pptv in the median (Q_1 : 91 pptv, Q_3 : 440 pptv) of the measured Cl_y is left unexplained by displacement from sea-salt particles with $D_p < 4 \mu\text{m}$.

Research Flight 3, which took place over the ocean and downwind of New York City, stands out in Figure 2c. On this flight, Cl_y had a median concentration of 714 pptv, reaching a maximum of 1,757 pptv over Manhattan with a median displaced chloride concentration of 294 pptv, leaving 420 pptv (Q_1 : 375 pptv, Q_3 : 568 pptv) of gas-phase Cl_y unexplained by displacement of chloride from PM_4 sea-salt particles. Even if only HCl, instead of total gas-phase Cl_y , is compared to dCl^- , the total amount of unexplained HCl is still 2 times greater, since HCl concentrations tend to dominate total Cl_y . The discrepancy is larger than uncertainties in Cl_y calibrations. Sampling aerosol in bulk is known to drive artificial displacement of HCl (Graedel & Keene, 1995), which would lead to an overestimate in dCl^- and, therefore, an underestimate in the amount of unexplained Cl_y shown in Figure 2c. Therefore, a filter sampling artifact is not responsible for the unexplained gas-phase Cl_y .

There are several reasons that the mass displaced from PM_4 sea salt below 1 km can explain only half of the gas-phase chlorine species measured during WINTER. One possible reason for the discrepancy is that the WINTER measurements of PM_4 are a truncated measurement of the sea-salt size distribution and thus an underestimate of available potential chloride mass (Keene et al., 1999). However, it remains questionable whether externally mixed particles $D_p > 4 \mu\text{m}$ contribute significantly to gas-phase HCl due to the greater buffering capacity. Most size-resolved estimates suggest the pH of these larger particles is higher than those in the submicron (Fang et al., 2017; Zaveri et al., 2008). That said, the degree to which coarse-mode chloride contributes to the displaced gas-phase Cl_y concentrations is not quantifiable with the WINTER measurements and will be challenging from any aircraft platform given the typical characteristic inlet cutoff sizes.

Finally, the unexplained source of gas-phase Cl_y could also be from anthropogenic sources. The areas sampled over the ocean with elevated Cl_y concentrations were downwind of major continental sources such as power plants in the Ohio River Valley and urban regions in the Washington DC-New York corridor, where other sources of chlorine compounds, such as the partitioning of gas-phase Cl_y compounds from road salt, could have been advected downwind that would enhance Cl_y emissions relative to pNa^+ concentrations, thereby increasing the amount of unexplained Cl_y . Research Flight 3, which saw the highest Cl_y concentrations and the largest amount unexplained by sea-salt displacement, took place 5 days after a major blizzard hit the Northeastern United States and on the night before another, such that the roads throughout the Northeastern United States were likely heavily salted. In addition, residential wood combustion was a ubiquitous aerosol source during WINTER (Schroder et al., 2018) and is known to emit pCl^- , often in the form of KCl (Reid et al., 2005). Figure 3a shows that the amount of unexplained Cl_y is positively correlated with carbon

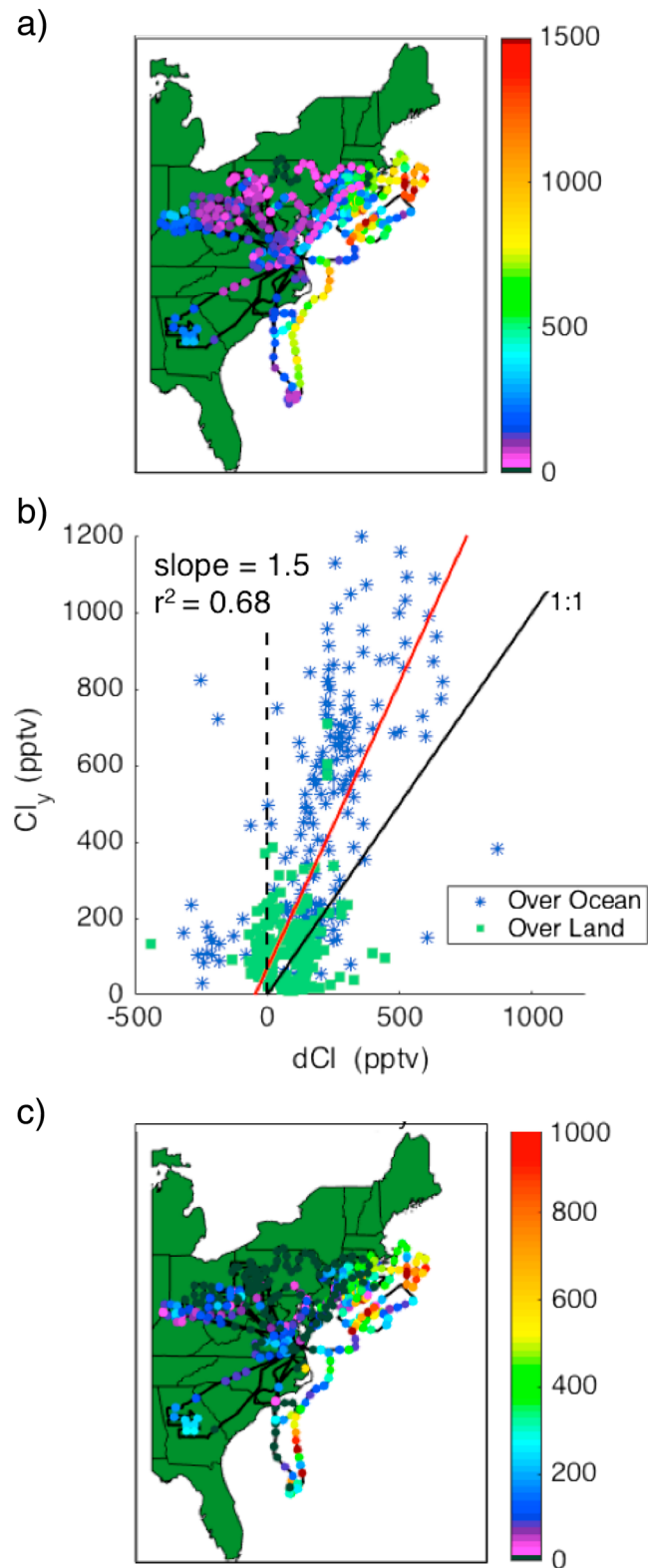


Figure 2. (a) Map showing the 5-min measurements of Cl_y (HCl + ClNO₂ + HOCl + Cl₂), colored by total mixing ratio (pptv). (b) The measured Cl_y is plotted versus the displaced mass of chloride from sea-salt particles, divided into those over the ocean and over land. (c) Map showing concentration of Cl_y that is not explained by displacement from sea salt ($Cl_y - dCl$). Flight tracks with insufficient data to calculate the unexplained Cl_y are shown as black lines.

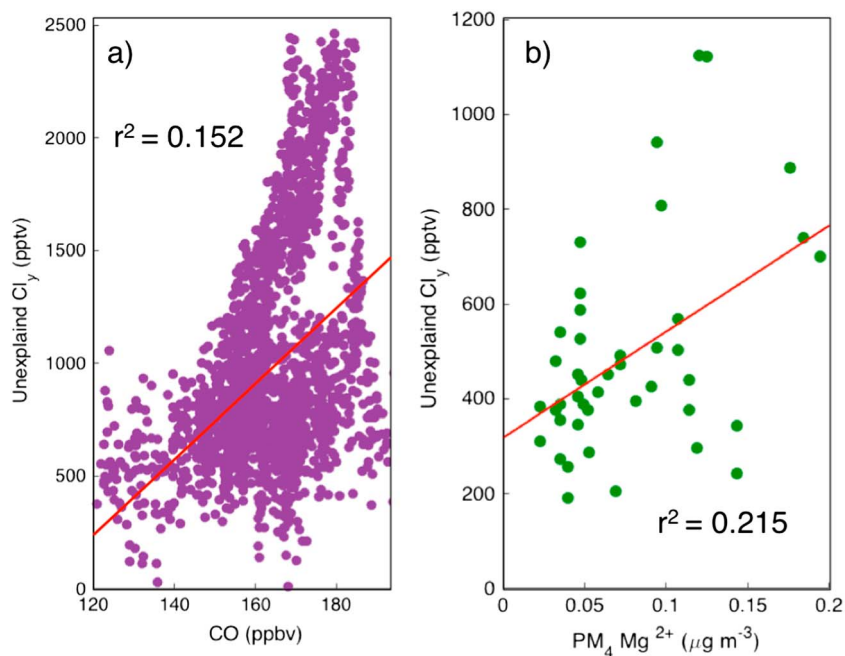


Figure 3. Measured relationship between the concentrations of Cl_y not explained by sea-salt displacement over the ocean below 1 km on Research Flight 3 and (a) CO at 10-s intervals and (b) pMg^{2+} at the University of New Hampshire filter intervals (5–7 min).

monoxide (CO) in areas over the ocean on this specific flight below 1,000 m ($r^2 = 0.152$). Similarly, we found that unexplained Cl_y was positively correlated ($r^2 = 0.22$) with UNH filter measurements of magnesium, a widely used component in road salt shown in Figure 3b. Therefore, some of the unexplained Cl_y could be from HCl that was displaced and advected downwind from an anthropogenic source of road salt on land that is not coemitted with pNa^+ . However, conclusive attribution is difficult in this regard because of the correlation that arises from transport of urban pollution tracers into the marine boundary layer where there is a natural chloride source.

Laskin et al. (2012) also found substantial chloride depletion in aged sea-salt particles that could not be explained by the known atmospheric reactivity of sea salt with inorganic nitric and sulfuric acids. They presented evidence that pCl^- may react with organic acids efficiently, releasing HCl gas to the atmosphere and leaving behind particles depleted in chloride and enriched in the corresponding organic salts. It is possible this mechanism could be occurring, especially in the coarse mode, depleting the aerosol chloride with respect to pNa^+ by displacing HCl.

3.2. ISORROPIA II Predictions of Chlorine Gas-Aerosol Partitioning

As shown in Figure 4, the Base ISORROPIA II simulation captures the observed $\text{HNO}_3\text{-NO}_3^-$ partitioning with a small underestimate in pNO_3^- of 8% on average with the RH dependence documented in Guo et al. (2016). The nitrate partitioning results shown here are not significantly different than those presented in Guo et al. (2016), indicating that the pH perturbation caused by adding reactive chloride as an ISORROPIA II input value is too small to affect nitrate partitioning. Similarly, the ammonia partitioning simulated here is not significantly different from that presented in Guo et al. (2016) for WINTER.

In the base simulation, ISORROPIA II tends to slightly underestimate the concentration of gas-phase HCl with a regression slope of 0.95. The degree to which ISORROPIA II can correctly predict HCl concentrations, well within the instrument uncertainty, lends confidence to the assumption that the HCl measured during the campaign is the equilibrium concentration, having equilibrated with the submicron aerosol populations. However, ISORROPIA II does overestimate the amount of pCl^- in the particle phase by a consistent factor of 2. The AMS rarely detected PM_1 pCl^- concentrations exceeding $0.2 \mu\text{g}/\text{m}^3$, despite ISORROPIA II predictions that at $\text{RH} > 80\%$, pCl^- could be as high as $0.5 \mu\text{g}/\text{m}^3$.

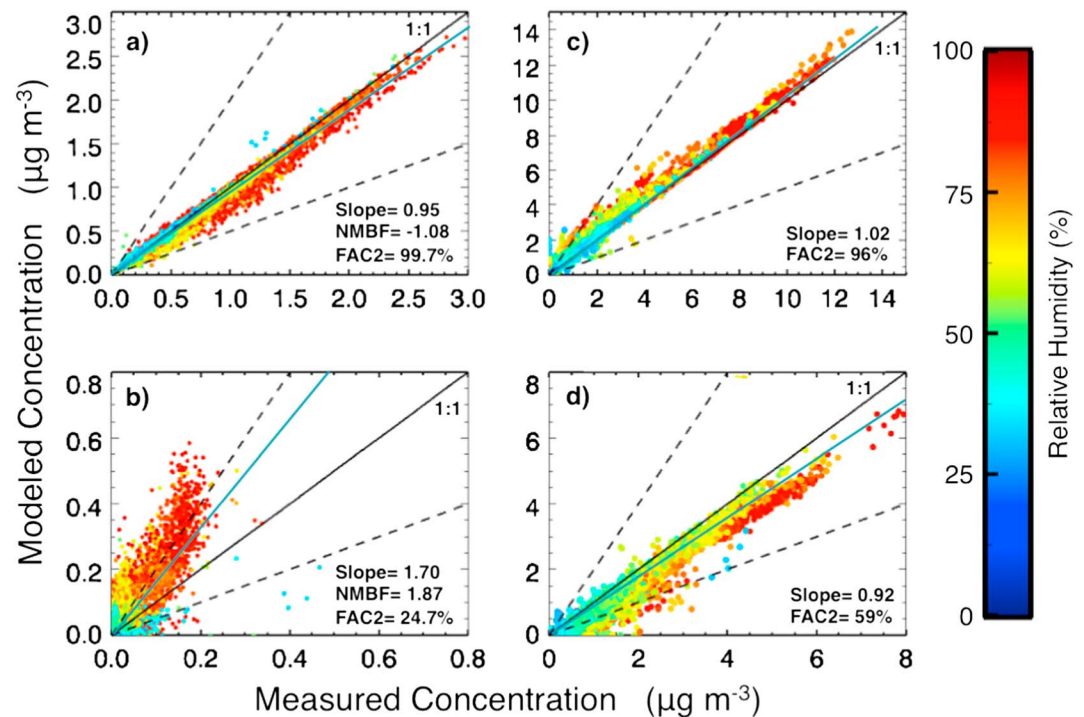


Figure 4. A comparison of ISORROPIA model-predicted and observed (a) gas-phase HCl, (b) particle chloride, and (c) gas-phase HNO_3 , and (d) particle nitrate, colored by relative humidity from the base simulation, including the line of best fit slope, number of points within a factor of 2 (FAC2), and the normalized mean bias factor (NMBF).

Several possible causes exist for ISORROPIA II's overestimate of PM_{10} pCl^- . First, we have inherently assumed that all the measured submicron, nonrefractory pCl^- is internally mixed with the measured submicron nitrate, ammonium, and sulfate. If this was not true, the pH of the externally mixed submicron aerosols that contain chloride would likely be higher than that calculated under our assumptions (Fang et al., 2017; Zaveri et al., 2008), in which case, the model would further shift HCl from the gas phase into the particle phase relative to the results presented here. This is the direction needed to match the observations and cannot be ruled out as a cause for this overprediction considering the measurements that were made during the WINTER campaign.

Second, the equilibrium model does not include nonequilibrium processes that remove chloride from the particle into the gas phase, such as ClNO_2 or Cl_2 production. However, presumably, if chloride was removed via other heterogeneous processes, the dynamic equilibrium for HCl and chloride would self-adjust. Finally, The AMS only observed nonrefractory pCl^- , which does not include that from PM_{10} sea salt. Therefore, another possible reason for the model-measurement disagreement shown in Figure 4 is that sea-salt chloride was not included in the total PM_{10} chloride input to ISORROPIA.

To investigate whether this possibility was a realistic cause for the observed model-measurement disagreement, we conducted a second ISORROPIA II simulation with an iterative addition of aqueous pNa^+ and pCl^- until the predicted gas-phase HCl matched the observed values, strictly requiring agreement within 15 pptv ($0.012 \mu\text{g/m}^3$). Not all points passed to ISORROPIA II needed an adjustment to total chloride to match the observed HCl. Therefore, the median concentration of pCl^- that had to be added to force chlorine-partitioning agreement was $0.0 \mu\text{g/m}^3$ for the whole campaign. Of the points that did require adjustment to total input chloride to match the observed HCl at $\text{RH} > 20\%$, the median pCl^- the AMS measured was $0.02 \mu\text{g/m}^3$, to which a median of $0.04 \mu\text{g/m}^3$ (Q_1 : $0.02 \mu\text{g/m}^3$, Q_3 : $0.06 \mu\text{g/m}^3$) of refractory chloride from sea salt had to be added. Therefore, the median total amount of refractory and nonrefractory chloride in the PM_{10} particles, where the partitioning did not initially match, was estimated to $0.07 \mu\text{g/m}^3$ (Q_1 : $0.04 \mu\text{g/m}^3$, Q_3 : $0.12 \mu\text{g/m}^3$). This analysis implies that in the median, we observed 35% of the total PM_{10} pCl^- with the AMS when sea salt was present in amounts appreciable enough to affect the chlorine partitioning.

It is important to note that the overall chlorine partitioning predicted by the model does not significantly change in the iterated NaCl simulation compared to the base simulation, as so little submicron sea salt is added in comparison to the concentrations of nitrate, sulfate, and ammonium that aerosol pH is negligibly changed. Therefore, we are comparing a nearly identical simulation of chlorine partitioning to a different measurement standard; the base simulation measurement comparison is only to nonrefractory chloride contributions to the particle phase and the iterated simulation allows for a small amount of internally mixed submicron sea salt.

To understand if the median total amount of refractory and nonrefractory pCl^- that is necessary for chlorine-partitioning agreement is a reasonable amount (in the median $0.07 \mu\text{g}/\text{m}^3$) that could be internally mixed, we compare the amount of additional pNa^+ and pCl^- to the other submicron particle chloride measurements and total particle mass. The DL of the PILS instrument on this time scale was $0.09 \mu\text{g}/\text{m}^3$ for PM_{10} pCl^- . Including measured values below the DL, the median PILS-measured amount of PM_{10} pCl^- was $0.06 \mu\text{g}/\text{m}^3$, while the UNH particle filters saw a median of $0.52 \mu\text{g}/\text{m}^3$ of pCl^- in PM_{4} including all observations. Therefore, in the median, the amount of total pCl^- required to be internally mixed for the ISORROPIA II HCl concentrations to match observations is lower than what the PILS could reliably detect, yet in good agreement with its median concentration, and requires only 12% the total PM_{4} pCl^- observed from the UNH filters to be present in internally mixed particles. The median amount of PM_{10} pNa^+ measured by the PILS fraction collector was $0.16 \mu\text{g}/\text{m}^3$, lower than what was added as NaCl for agreement, suggesting that only 25% of the submicron pNa^+ measured ($0.16 \mu\text{g}/\text{m}^3$) would have to be internally mixed for the measurement bias of the AMS chloride to be responsible for the ISORROPIA II model-measurement disagreement shown in Figure 4.

Research Flight 3 required the most pCl^- to be added to bring the model into agreement with the measurements and showed elevated levels of all gas-phase Cl₂ compounds and AMS pCl^- . This specific flight took place off the coast of New York City on the night of 7 February 2015 and followed a polluted plume below 2 km as it aged through dusk into the night and is used as a case study to verify that the chlorine-partitioning discrepancy can be explained by a fraction of unmeasured pCl^- . Figure 5a shows the base simulation's predicted and observed chlorine partitioning. For this specific flight, only 39.4% of ISORROPIA II calculated pCl^- was within a factor of 2 of the measurements in the base simulation, with ISORROPIA II consistently overpredicting the observed pCl^- . The uncertainty in the pCl^- and HCl measurements and the model response to those uncertainties were not enough to explain the model-measurement discrepancy observed. For this flight, the nitrate partitioning showed model agreement always within the measurement uncertainty.

Figure 5b shows the same time series for Research Flight 3 for the iterated NaCl simulation. By design, 100% of the predictions fall within 15 pptv of observed HCl. A median of $0.04 \mu\text{g}/\text{m}^3$ (Q_1 : $0.03 \mu\text{g}/\text{m}^3$, Q_3 : $0.07 \mu\text{g}/\text{m}^3$) of refractory chloride from sea salt had to be added to the median of $0.08 \mu\text{g}/\text{m}^3$ pCl^- measured by the AMS for a total of $0.12 \mu\text{g}/\text{m}^3$ (Q_1 : $0.07 \mu\text{g}/\text{m}^3$, Q_3 : $0.20 \mu\text{g}/\text{m}^3$) of internally mixed pCl^- in the median to sustain the observed HCl concentrations in equilibrium. Coincidentally, this flight recorded the highest HCl concentrations in the marine boundary layer.

Figure 5c shows all three different measurements of pCl^- from Research Flight 3 compared to the amount required for agreement with ISORROPIA II predictions. The amount of added chloride is larger than the amount observed by the AMS, comparable to that measured by the PILS, and lower than the UNH filter measurements of pCl^- . A median of $0.61 \mu\text{g}/\text{m}^3$ of PM_{4} from the filters, likely only a fraction of the total amount of supermicron chloride, was observed on this flight, and we require only $0.12 \mu\text{g}/\text{m}^3$ to be present in internally mixed particles to explain the observed chlorine partitioning. Thus, for this flight, contributions to total chloride from submicron sea-salt particles, which the AMS would not sample, could not be ruled out as a reason for the observed partitioning discrepancy.

To explore this possibility further, we use the particle size distribution measurements made aboard the aircraft to estimate the amount of mass in particles with a diameter less than $2.5 \mu\text{m}$ that could be present as internally mixed particles and contributing to equilibrium chlorine partitioning but would not be measured by the AMS due to the inlet cutoff of $1 \mu\text{m}$. Figure 6a shows the median mass distribution for Research Flight 3 from the PCASP by assuming a constant, intentionally conservative particle density of $1 \text{ g}/\text{cm}^3$. Figure 6b shows the time series of the integrated particle mass concentration from particles with a wet

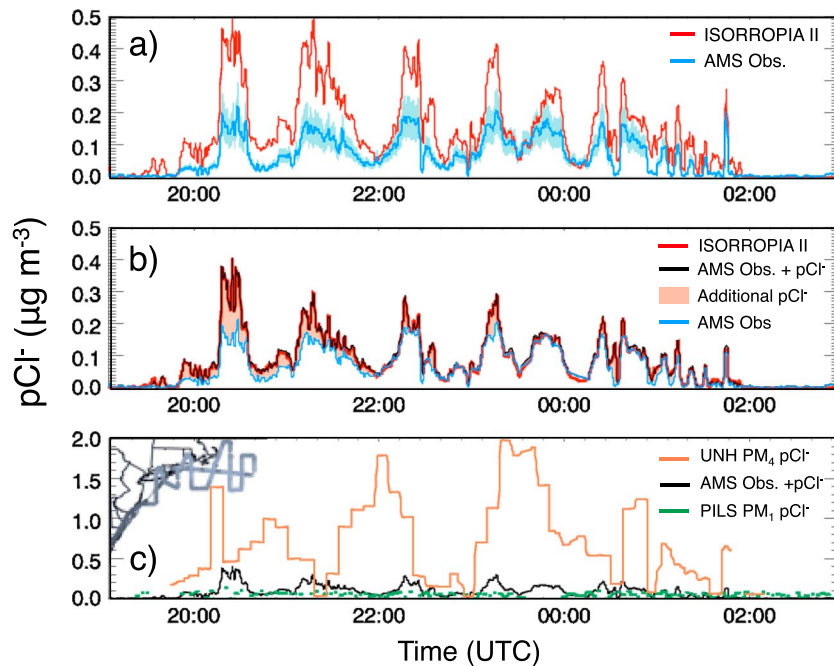


Figure 5. Time series of predicted and observed chlorine species from Research Flight 3, off the coast of New York City on the night of 7 February 2015. (a) The Base ISORROPIA II simulation-predicted pCl⁻ concentrations (red) compared to the AMS observations (blue) with measurement uncertainty shown as shading. (b) The iterated NaCl simulation-predicted pCl⁻ concentrations (red) compared to the observed pCl⁻ concentrations (blue), adjusted by an added hypothetical NaCl component (orange shading) that brings the measured and predicted HCl (g) into agreement (black). (c) The total amount of pCl⁻ needed to match the chlorine partitioning in the iterated NaCl simulation (black) compared to water-soluble chloride measured by the PILS (green) and PM₄ pCl⁻ measured by the UNH filters (orange), and an inset of the Research Flight 3 flight track. AMS = aerosol mass spectrometer; PILS = particle-into-liquid sampler; UNH = University of New Hampshire.

diameter <2.5 μm derived from the PCASP and compares this to the amount of iterated NaCl needed to force the chlorine-partitioning agreement and to the amount of pNa⁺ measured by the PILS fraction collector. The amount of iterated pNa⁺ added is either in good agreement with the amount of measured PILS pNa⁺ or less than what was measured. This comparison shows that although this flight required the largest amount of chloride to be added to explain the partitioning, there is likely sufficient pCl⁻ mass available in particles with sizes less than 2.5 μm that would be equilibrating with the gas phase but potentially unmeasured by the available composition instrumentation.

3.3. Effective Equilibrium Constant

The above simulations inherently assume that the equilibrium constant used in ISORROPIA II for HCl partitioning to aerosol is correct. The discrepancies observed in chlorine partitioning, however, could be due to a variety of thermodynamic inconsistencies in the model including the aerosol mixing state, Henry's law constant, acid dissociation constant, activity coefficient parameterizations, and their temperature dependencies, instead of just a lack of measured refractory chloride. The measured fraction of total chlorine in the particle phase ($f_p(\text{Cl}) = \text{AMS pCl}^- / [\text{AMS pCl}^- + \text{CIMS HCl}]$) as a function of the ISORROPIA II-predicted pH from the base simulation is shown in Figure 7a, colored by observed RH, which is a proxy for aerosol liquid water content. The ISORROPIA II predictions of $f_p(\text{Cl})$ follow an exponential relationship with [H⁺] (Figure 7b), as expected. The observed $f_p(\text{Cl})$ (Figure 7a) also somewhat follows an exponential trend with pH, but at a lower overall magnitude. ISORROPIA II overpredicts $f_p(\text{Cl})$ at higher pH, and at extremely low pH (<0.25), the scatter and divergence in the observations (Figure 7a) from the ideal modeled behavior (Figure 7b) increases. The tendency of the model to underestimate pCl⁻ at extremely low pH and overestimate it at pH >0.5 is seen more clearly in measurement-model difference shown in Figure 7c. The model predicts that no pCl⁻ can exist at pH <0, regardless of how much water is present in the particle (governed by ambient RH), but the observations show that pCl⁻ is rarely zero, even at predicted pH <0.25.

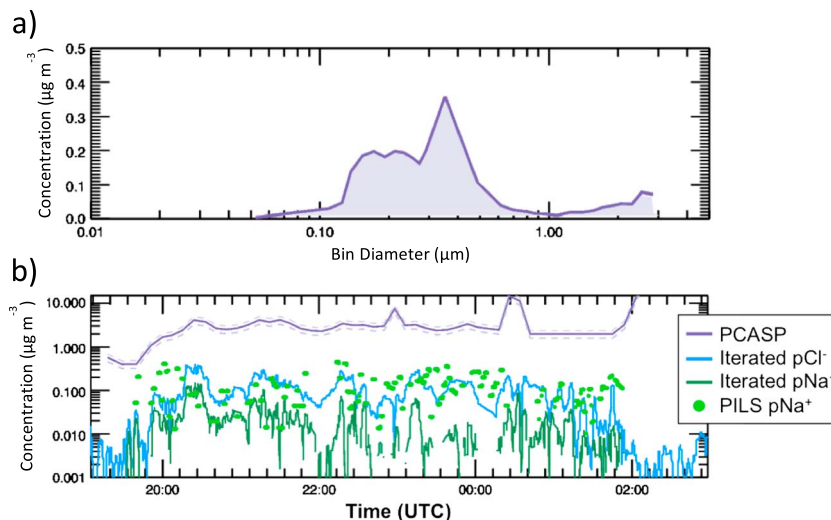


Figure 6. (a) Median particle mass distribution in time from the PCASP for Research Flight 3, highlighting the mass contained in particles with wet diameter less than 2.5 μm . (b) A time series of the additional pNa^+ and pCl^- from the iterated NaCl (which added to the AMS observations), compared to the PILS pNa^+ fraction collector data and the median integrated mass from particles with a wet diameter less than 2.5 μm determined from the PCASP with the instrument uncertainty shown as a dashed line. See text for details. PCASP = Passive Cavity Aerosol Spectrometer Probe; AMS = aerosol spectrometer; PILS = particle-into-liquid sampler.

The trends highlighted in Figure 7 suggest that decreasing ideality at low pH affects chloride partitioning more strongly than described by the current parameterization of the activity coefficients. The points in Figure 7c are sized by their activity coefficients and colored by the ambient RH. The model-measurement discrepancy trend is clearly greater for very humid points with large activity coefficients. Noticeably, in Figure 7c, the model underpredicts particle chloride for points at $\text{pH} < 0.5$ while overpredicting those at $\text{pH} > 0.5$, with a tendency toward worse agreement for points with high activity coefficients and high RH. Figure 7d shows that the parameterized activity coefficients from ISORROPIA II increase exponentially at $\text{pH} < 0.5$ for points with high RH, as documented in Fountoukis et al. (2009). This large change in activity coefficients ultimately drives the modeled pCl^- to zero at low pH, by correcting for the nonideality of a solution with a pH so low. In the pH range relevant for accurately assessing chloride partitioning, the parameterized activity coefficients can vary across an entire order of magnitude at the same predicted pH for different RH with considerable uncertainty at low temperatures. It is possible, given the large uncertainty range in the activity coefficient values for conditions typical in submicron atmospheric aerosols, that the activity coefficients themselves are responsible for the model-measurement disagreement presented herein (Fountoukis & Nenes, 2007) rather than a measurement issue or problem of definition (i.e., externally mixed NaCl) as discussed above. We compared the activity coefficients from ISORROPIA II, known to sacrifice some accuracy for computational speed, to those predicted by the Extended Aerosol Inorganics Model (E-AIM) IV (Friese & Ebel, 2010) and saw that the predicted activity coefficients were comparable at typical WINTER conditions for $\text{pH} > 0.5$ but tended to diverge further from one another as pH decreased with E-AIM predicting higher activity coefficients. At such low pH, the activity coefficients predicted by both E-AIM and ISORROPIA II are larger than 1; under what conditions, neither predicts that any particle chloride can exist, despite observations that submicron particles are rarely completely depleted in Cl^- . Therefore, this divergence in predicted coefficients at low pH does not impact the results presented here. At higher pH, the activity coefficients are in much better agreement with one another (± 0.06), though E-AIM's predicted chlorine partitioning is slightly better than ISORROPIA II's given its larger activity coefficients. However, in the median, E-AIM still overpredicts the amount of chloride present in the particle phase by factor of approximately 2.

For comparison with past and future studies, we derive an implied equilibrium constant from the WINTER data by using ISORROPIA II to predict the particle pH, liquid water content, and activity coefficients. Figure 8a shows the comparison of the WINTER data's implied equilibrium constant when the base

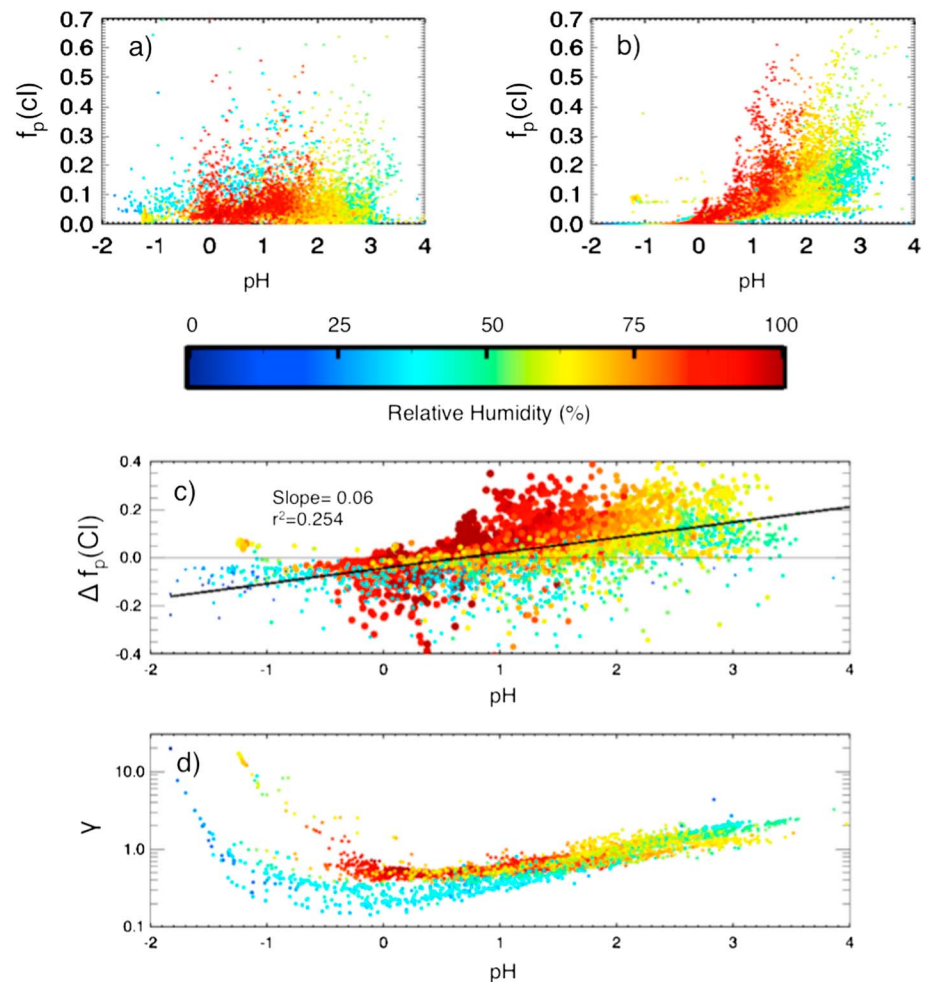


Figure 7. (a) The observed particle-phase fraction of chloride ($f_p(\text{Cl})$) as a function of model-predicted pH and colored by relative humidity (RH) for the base simulation. (b) Model-predicted $f_p(\text{Cl})$ for the base simulation colored by RH. (c) The difference between model and measured $f_p(\text{Cl})$ as a function of pH and sized by their activity coefficients and colored by RH. (d) The activity coefficients parameterized by the model as a function of pH and colored by RH.

simulation-predicted pH, liquid water content, and activity coefficients are used with the CIMS HCl measurement and high-resolution time-of-flight AMS PM_{10} chloride measurement in the following expression:

$$K_{\text{eq}} = \frac{[\text{H}^+][\text{Cl}^-]}{[\text{HCl}]} \left(\frac{\gamma_{\text{Cl}}}{\text{LWC}} \right)^2$$

where K_{eq} is in units of $\text{mol}^2 \cdot \text{kg}_{\text{soln}}^{-2} \cdot \text{atm}^{-1}$, $[\text{H}^+]$ and $[\text{Cl}^-]$ are in mol/m^3 , $[\text{HCl}]$ in atm, LWC (liquid water content) is in units of kg/m^3 , and γ_{Cl} is unitless. Henry's law data compiled for HCl were drawn from Sander (2015). If the original publication derived no acid dissociation constant, then that of Marsh and McElroy (1985) was used to determine an equilibrium constant. By fitting an exponential to the median of the data binned by temperature during the WINTER campaign, a function was derived that represents the median equilibrium constant observed during WINTER. Shown in black in Figure 8b, the observation-based equilibrium constant function was found to be

$$K_{\text{eq}} = 2.5 \times 10^6 \exp \left[5208 \left(\frac{1}{T} - \frac{1}{298} \right) \right] \quad (\text{mol}^2 \cdot \text{kg}_{\text{soln}}^{-2} \cdot \text{atm}^{-1})$$

This function was derived from the 10-s ISORROPIA II base simulation and WINTER measurements and excludes points with activity coefficients greater than 1, predicted pH < 0.5, HCl < 100 pptv, $\text{pCl}^- < 0.01 \mu\text{g}/\text{m}^3$, RH < 20%, and pressure altitude < 1,000 m. This function does not significantly change the

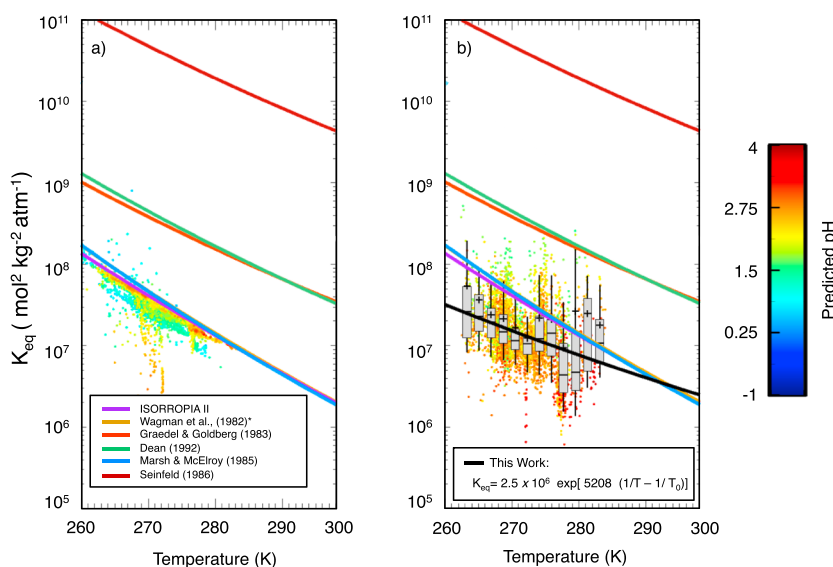


Figure 8. (a) The implied equilibrium constant as a function of temperature, colored by pH from the outputted ISORROPIA II HCl and Cl^- concentrations, pH, LWC, and activity from the iterated NaCl simulation compared to literature functions (lines) assuming activity coefficients equal to 1. (b) The implied equilibrium constant as a function of temperature, colored by predicted pH, from the measured HCl and Cl^- concentrations during WINTER and ISORROPIA II-predicted pH, LWC, and activity coefficients from the base simulation. Box and whisker plots show the medians of data within a selected temperature range. For information on Henry's law constants and acid dissociation constants used to derive the listed functions, see Wagman et al. (1982), Graedel and Goldberg (1983), Dean (1992), Marsh and McElroy (1985), and Seinfeld (1986). *Function also derived in Brimblecombe and Clegg (1989) and Carslaw et al. (1995). LWC = liquid water content; WINTER = Wintertime Investigation of Transport, Emissions, and Reactivity.

implied value of the equilibrium constant at 298 K, suggesting a slightly higher value than that currently in ISORROPIA II (changing from $1.916 \times 10^6 \text{ mol}^2 \cdot \text{kg}_{\text{soln}}^{-2} \cdot \text{atm}^{-1}$ to $2.5 \times 10^6 \text{ mol}^2 \cdot \text{kg}_{\text{soln}}^{-2} \cdot \text{atm}^{-1}$), which is well within the range of published values. However, the WINTER data are heavily weighted to observing conditions at lower temperatures ($T < 275 \text{ K}$), not temperatures close to 298 K where most previous functions were derived. The WINTER data suggest a lower temperature dependence of the equilibrium function of 5208 K^{-1} compared to the published literature values of $\sim 6800\text{--}9200 \text{ K}^{-1}$. This temperature dependence reflects the combination of those in Henry's law and acid dissociation constants.

It should be noted that this function was derived using chloride measurements that do not contain contributions from potentially unmeasured sea salt and would not be expected to be the true partitioning function. If the true amount of pCl^- in particles were larger than what was measured by the AMS, as we have presented evidence of, then the implied equilibrium constant would increase, thereby bringing it into closer agreement with published literature functions. Thus, our value is an observationally constrained lower limit of the effective equilibrium constant for HCl.

As Figure 8b demonstrates, in PM_{10} aerosols with low pH and small volumes, the value of the activity coefficients is enough to push the effective equilibrium constant throughout 2 orders of magnitude. Therefore, how activity coefficients are parameterized in highly nonideal solutions will ultimately impact our ability to constrain this value any further, even with improved measurements of the full range of pCl^- , and the application of ISORROPIA II to such unideal mixtures should be done with the caution.

4. Summary

We present speciated reactive chlorine observations (HCl, pCl^- , HOCl, ClNO_2 , and Cl_2) obtained during the WINTER campaign aboard the NCAR C-130 aircraft from February to March 2015. Over both the ocean and land, the measured inorganic chlorine compounds were dominated by gas-phase HCl and PM_{10} pCl^- . The total amount of all measured inorganic chlorine compounds was greater than 2 times larger over the ocean than over land within the bottom 1 km of the atmosphere. Elevated levels of HCl (g), routinely upward of

300 pptv, are seen below 1 km over the ocean, whereas over-land concentrations of HCl were typically 100 pptv, except near power plant plumes where HCl concentrations exceeded 1 ppbv. We observed ClNO₂ peaking at night at over the ocean with a concentration of 119 pptv in the median, below 1 km; however, we sampled plumes offshore over the ocean that peaked >1,000 pptv of ClNO₂ and which lasted well into the early morning until nearly 10 a.m. local time. In the median, we observed 3.7 pptv of ClNO₂ over land, but we observed localized plumes upward of 70 pptv at night, which is enough to significantly impact the morning radical budget in the winter (Riedel et al., 2013). We observed HOCl concentrations of 3.4–3.9 pptv in the median within 1 km over the ocean, with generally lower concentrations of HOCl in the polluted air sampled during WINTER than were sampled in the pristine marine air during the Cape Verde campaign presented in Lawler et al. (2011).

AMS observations show 0–20% of available total nonrefractory chlorine partitions into the PM₁ particles (0–0.2 μg/m³_{amb}) at sufficiently high RH, low temperatures, and pH above 0.5. The ISORROPIA II thermodynamic model of the system initially correctly predicted HCl concentrations with a regression slope of 1.05 but over-predicted submicron pCl[−] by about a factor 2 when pH was >0.5. This discrepancy could be explained by small amounts of refractory chloride, such as sea-salt particles, that the AMS pCl[−] measurement would not capture but that could be fully or partially in equilibrium with gas-phase HCl. The amount of additional NaCl needed to explain the model-measurement difference was less than the total observed PM₄ pCl[−] mass concentration, less than the submicron pNa⁺ measured by the PILS fraction collector, and well below the range of total mass concentration derived from the measured number concentrations of particles with D_p < 1 μm.

Large uncertainties in the parameterized activity coefficients typical for systems with pH <0.5 and low RH ultimately limit the validity of chloride-partitioning calculations under those conditions, as previously noted in Fountoukis and Nenes (2007). Based on the measurement-model difference in the particle-phase fraction of chloride, we derive a lower limit to the effective equilibrium constant for HCl to be K_{eq} = 2.5 × 10⁶ exp[5,208 (1/T − 1/T₀) mol²·kg_{soln}^{−2}·atm^{−1}]. This value suggests a slight decrease in the temperature dependency of the HCl effective equilibrium constant function used in ISORROPIA II. This work highlights the sensitivity of chlorine partitioning in ISORROPIA II to even minor input changes and demonstrates that the equilibrium constant may not be able to be further constrained by field data in highly unideal, cold particles unless parameterizations of activity coefficients in this extreme are better defined or lower DLs for water-soluble NaCl can be made. Refinements to our representation of the basic thermodynamic parameters used in partitioning models and to instrumentation to measure pCl[−] will be necessary to dynamically simulate atmospheric halogen chemistry.

Acknowledgments

This work was supported by U.S. Environmental Protection Agency (EPA) STAR grant FP-91780601-0 to J. D. H. and the National Science Foundation (NSF) under grant AGS-1360745 to J. A. T. as part of the WINTER aircraft campaign with support from the National Oceanic and Atmospheric Administration's Earth System Research Laboratory. The WINTER data are provided by NCAR/EOL under sponsorship of the NSF (<http://data.eol.ucar.edu>). The CU-Boulder group was supported by NSF AGS-1360834 and National Aeronautics and Space Administration (NASA) NNX15AT96G.

References

- Ansari, A. S., & Pandis, S. N. (2000). The effect of metastable equilibrium states on the partitioning of nitrate between the gas and aerosol phases. *Atmospheric Environment*, 34(1), 157–168. [https://doi.org/10.1016/S1352-2310\(99\)00242-3](https://doi.org/10.1016/S1352-2310(99)00242-3)
- Bahreini, R., Dunlea, E. J., Matthew, B. M., Simons, C., Docherty, K. S., DeCarlo, P. F., et al. (2008). Design and operation of a pressure-controlled inlet for airborne sampling with an aerodynamic aerosol lens. *Aerosol Science and Technology*, 42(6), 465–471. <https://doi.org/10.1080/02786820802178514>
- Bannan, T. J., Booth, A. M., Bacak, A., Muller, J. B. A., Leather, K. E., Le Breton, M., et al. (2015). The first UK measurements of nitryl chloride using a chemical ionization mass spectrometer in Central London in the summer of 2012, and an investigation of the role of Cl atom oxidation. *Journal of Geophysical Research: Atmospheres*, 120, 5638–5657. <https://doi.org/10.1002/2014JD022629>
- Behnke, W., George, C., Scheer, V., & Zetzsch, C. (1997). Production and decay of ClNO₂ from the reaction of gaseous N₂O₅ with NaCl solution: Bulk and aerosol experiments. *Journal of Geophysical Research*, 102(D3), 3795–3804. <https://doi.org/10.1029/96JD03057>
- Bertram, T. H., & Thornton, J. A. (2009). Toward a general parameterization of N₂O₅ reactivity on aqueous particles: The competing effects of particle liquid water, nitrate and chloride. *Atmospheric Chemistry and Physics*, 9(21), 8351–8363. <https://doi.org/10.5194/acp-9-8351-2009>
- Brimblecombe, P., & Clegg, S. L. (1989). Erratum. *Journal of Atmospheric Chemistry*, 8, 95.
- Canagaratna, M. R., Jayne, J. T., Jimenez, J. L., Allan, J. D., Alfarra, M. R., Zhang, Q., et al. (2007). Chemical and microphysical characterization of ambient aerosols with the aerodyne aerosol mass spectrometer. *Mass Spectrometry Reviews*, 26(2), 185–222. <https://doi.org/10.1002/mas.20115>
- Carslaw, K. S., Clegg, S. L., & Brimblecombe, P. (1995). A thermodynamic model of the system HCl-HNO₃-H₂SO₄-H₂O, including solubilities of HBr, from <200 to 328K. *The Journal of Physical Chemistry*, 99(29), 11,557–11,574. <https://doi.org/10.1021/j100029a039>
- Dean, J. A. (1992). *Lange's handbook of chemistry*. New York, NY: McGraw-Hill, Inc.
- DeCarlo, P. F., Kimmel, J. R., Trimborn, A., Northway, M. J., Jayne, J. T., Aiken, A. C., et al. (2006). Field-deployable, high-resolution, time-of-flight aerosol mass spectrometer. *Analytical Chemistry*, 78(24), 8281–8289. <https://doi.org/10.1021/ac061249n>
- Dibb, J. E., Talbot, R. W., & Scheuer, E. M. (2000). Composition and distribution of aerosols over the North Atlantic during the Subsonic Assessment Ozone and Nitrogen Oxide Experiment (SONEX). *Journal of Geophysical Research*, 105(D3), 3709–3717. <https://doi.org/10.1029/1999JD000424>

- Dibb, J. E., Talbot, R. W., Scheuer, E. M., Blake, D. R., Blake, N. J., Gregory, G. L., et al. (1999). Aerosol chemical composition and distribution during the Pacific Exploratory Mission (PEM) Tropics. *Journal of Geophysical Research*, *104*(D5), 5785–5800. <https://doi.org/10.1029/1998JD100001>
- Fang, T., Guo, H., Zeng, L., Verma, V., Nenes, A., & Weber, R. J. (2017). Highly acidic ambient particles, soluble metals, and oxidative potential: A link between sulfate and aerosol toxicity. *Environmental Science & Technology*, *51*(5), 2611–2620. <https://doi.org/10.1021/acs.est.6b06151>
- Faxon, C., Bean, J., & Hildebrandt-Ruiz, L. (2015). Inland concentrations of ClNO₂ in Southeast Texas suggest chlorine chemistry significantly contributes to atmospheric reactivity. *Atmosphere*, *6*, 1487–1506. <https://doi.org/10.3390/atmos6101487>
- Finlayson-Pitts, B., Ezell, M., & Pitts, J. (1989). Formation of chemically active chlorine compounds by reactions of atmospheric NaCl particles with gaseous N₂O₅ and ClONO₂. *Nature*, *337*(6204), 241–244. <https://doi.org/10.1038/337241a0>
- Fountoukis, C., & Nenes, A. (2007). ISORROPIA II: A computationally efficient thermodynamic equilibrium model for K⁺–Ca²⁺–Mg²⁺–NH₄⁺–Na⁺–SO₄²⁻–NO₃⁻–Cl⁻–H₂O aerosols. *Atmospheric Chemistry Physics*, *7*, 4639–4659. <https://doi.org/10.5194/acp-7-4639-2007>
- Fountoukis, C., Nenes, A., Sullivan, A., Weber, R., Van Reken, T., Fischer, M., et al. (2009). Thermodynamic characterization of Mexico City aerosol during MILAGRO 2006. *Atmospheric Chemistry and Physics*, *9*(6), 2141–2156. <https://doi.org/10.5194/acp-9-2141-2009>
- Friese, E., & Ebel, A. (2010). Temperature dependent thermodynamic model of the system H⁺–NH₄⁺–Na⁺–SO₄²⁻–NO₃⁻–Cl⁻–H₂O. *The Journal of Physical Chemistry A*, *114*(43), 11,595–11,631. <https://doi.org/10.1021/jp101041j>
- Graedel, T. E., & Goldberg, K. I. (1983). Kinetic studies of raindrop chemistry: Inorganic and organic processes. *Journal of Geophysical Research*, *88*(C15), 10,865–10,882. <https://doi.org/10.1029/JC088iC15p10865>
- Graedel, T. E., & Keene, W. C. (1995). Tropospheric budget of reactive chlorine. *Global Biogeochemical Cycles*, *9*(1), 47–77. <https://doi.org/10.1029/94GB03103>
- Guo, H., Liu, J., Froyd, K. D., Roberts, J. M., Veres, P. R., Hayes, P. L., Jimenez, J. L., et al. (2017). Fine particle pH and gas–particle phase partitioning of inorganic species in Pasadena, California, during the 2010 CalNex campaign. *Atmospheric Chemistry and Physics*, *17*(9), 5703–5719. <https://doi.org/10.5194/acp-17-5703-2017>
- Guo, H., Sullivan, A. P., Campuzano-Jost, P., Schroder, J. C., Lopez-Hilfiker, F. D., Dibb, J. E., et al. (2016). Fine particle pH and the partitioning of nitric acid during winter in the Northeastern United States. *Journal of Geophysical Research: Atmospheres*, *121*, 10,355–10,376. <https://doi.org/10.1002/2016JD025311>
- Guo, H., Xu, L., Bougiatioti, A., Cerully, K. M., Capps, S. L., Hite, J. R., et al. (2015). Fine-particle water and pH in the southeastern United States. *Atmospheric Chemistry and Physics*, *15*(9), 5211–5228. <https://doi.org/10.5194/acp-15-5211-2015>
- Hayes, P. L., Ortega, A. M., Cubison, M. J., Froyd, K. D., Zhao, Y., Cliff, S. S., et al. (2013). Organic aerosol composition and sources in Pasadena, California, during the 2010 CalNex campaign. *Journal of Geophysical Research: Atmospheres*, *118*, 9233–9257. <https://doi.org/10.1002/jgrd.50530>
- Jayne, J. T., Leard, D. C., Zhang, X., Davidovits, P., Smith, K. A., Kolb, C. E., & Worsnop, D. R. (2000). Development of an aerosol mass spectrometer for size and composition analysis of submicron particles. *Aerosol Science and Technology*, *33*(1–2), 49–70. <https://doi.org/10.1080/027868200410840>
- Junge, C., & Werby, R. T. (1958). Concentration of chloride, sodium, potassium, calcium, and sulfate in rain water over the United States. *Journal of Meteorology*, *15*(5), 417–425. [https://doi.org/10.1175/1520-0469\(1958\)015<0417:TCOCSP>2.0.CO;2](https://doi.org/10.1175/1520-0469(1958)015<0417:TCOCSP>2.0.CO;2)
- Keene, W. C., Aslam, M., Khalil, K., Erickson, D. J. III, McCulloch, A., & Graedel, T. E. (1999). Composite global emissions of reactive chlorine from anthropogenic and natural sources: Reactive Chlorine Emissions Inventory. *Journal of Geophysical Research*, *104*(D7), 8429–8440. <https://doi.org/10.1029/1998JD100084>
- Keene, W. C., Stutz, J., Pszenny, A. A. P., Maben, J. R., Fischer, E. V., Smith, A. M., et al. (2007). Inorganic chlorine and bromine in coastal New England air during summer. *Journal of Geophysical Research*, *112*, D10S12. <https://doi.org/10.1029/2006JD007689>
- Kimmel, J. R., Farmer, D. K., Cubison, M. J., Sueper, D., Tanner, C., Nemitz, E., et al. (2011). Real-time aerosol mass spectrometry with millisecond resolution. *International Journal of Mass Spectrometry*, *303*(1), 15–26. <https://doi.org/10.1016/j.ijms.2010.12.004>
- Laskin, A., Moffet, R. C., Gilles, M. K., Fast, J. D., Zaveri, R. A., Wang, B., et al. (2012). Tropospheric chemistry of internally mixed sea salt and organic particles: Surprising reactivity of NaCl with weak organic acids. *Journal of Geophysical Research*, *117*, D15302. <https://doi.org/10.1029/2012JD017743>
- Lawler, M. J., Sander, R., Carpenter, L. J., Lee, J. D., Von Glasow, R., Sommariva, R., & Saltzman, E. S. (2011). HOCl and Cl₂ observations in marine air. *Atmospheric Chemistry and Physics*, *11*(15), 7617–7628. <https://doi.org/10.5194/acp-11-7617-2011>
- Lee, B. H., Lopez-Hilfiker, F. D., Mohr, C., Kurten, T., Worsnop, D. R., & Thornton, J. A. (2014). An iodide-adduct high-resolution time-of-flight chemical-ionization mass spectrometer: Application to atmospheric inorganic and organic compounds. *Environmental Science & Technology*, *48*(11), 6309–6317. <https://doi.org/10.1021/es500362a>
- Lee, B. H., Lopez-Hilfiker, F. D., Veres, P. R., McDuffie, E. M., Fibiger, D. L., Sparks, T. L., et al. (2018). Flight deployment of a high-resolution time-of-flight chemical ionization mass spectrometer: Observations of reactive halogen and nitrogen oxide species. *Journal of Geophysical Research: Atmospheres*, *123*, 7670–7686. <https://doi.org/10.1029/2017JD028082>
- Lopez-Hilfiker, F. D., Iyer, S., Mohr, C., Lee, B. H., D'Ambro, E. L., Kurtén, T., & Thornton, J. A. (2016). Constraining the sensitivity of iodide adduct chemical ionization mass spectrometry to multifunctional organic molecules using the collision limit and thermodynamic stability of iodide ion adducts. *Atmospheric Measurement Techniques*, *9*(4), 1505–1512. <https://doi.org/10.5194/amt-9-1505-2016>
- Malm, W. C., & Day, D. E. (2001). Estimates of aerosol species scattering characteristics as a function of relative humidity. *Atmospheric Environment*, *35*(16), 2845–2860. [https://doi.org/10.1016/S1352-2310\(01\)00077-2](https://doi.org/10.1016/S1352-2310(01)00077-2)
- Marsh, A. R. W., & McElroy, W. J. (1985). The dissociation constant and Henry's law constant of HCl in aqueous solution. *Atmospheric Environment*, *19*(7), 1075–1080. [https://doi.org/10.1016/0004-6981\(85\)90192-1](https://doi.org/10.1016/0004-6981(85)90192-1)
- McNaughton, C., Clarke, A. D., Howell, S. G., Pinkerton, M., Anderson, B., Thornhill, L., et al. (2007). Results from the DC-8 inlet characterization experiment (DICE): Airborne versus surface sampling of mineral dust and sea salt aerosols. *Aerosol Science and Technology*, *41*(2), 136–159. <https://doi.org/10.1080/02786820601118406>
- Mielke, L. H., Furgeson, A., & Osthoff, H. D. (2011). S.I.: Observation of ClNO₂ in a mid-continental urban environment. *Environmental Science & Technology*, *45*(20), 8889–8896. <https://doi.org/10.1021/es201955u>
- Mielke, L. H., Stutz, J., Tsai, C., Hurlock, S. C., Roberts, J. M., Veres, P. R., et al. (2013). Heterogeneous formation of nitryl chloride and its role as a nocturnal NO_x reservoir species during CalNex-LA 2010. *Journal of Geophysical Research: Atmospheres*, *118*, 10,638–10,652. <https://doi.org/10.1002/jgrd.50783>
- Osthoff, H. D., Roberts, J. M., Ravishankara, A. R., Williams, E. J., Lerner, B. M., Sommariva, R., et al. (2008). High levels of nitryl chloride in the polluted subtropical marine boundary layer. *Nature Geoscience*, *1*(5), 324–328. <https://doi.org/10.1038/ngeo177>
- Phillips, G. J., Tang, M. J., Thieser, J., Brickwedde, B., Schuster, G., Bohn, B., et al. (2012). Significant concentrations of nitryl chloride observed in rural continental Europe associated with the influence of sea salt chloride and anthropogenic emissions. *Geophysical Research Letters*, *39*, L10811. <https://doi.org/10.1029/2012GL051912>

- Reid, J. S., Koppmann, R., Eck, T. F., & Eleuterio, D. P. (2005). A review of biomass burning emissions part II: Intensive physical properties of biomass burning particles. *Atmospheric Chemistry and Physics*, 5(3), 799–825. <https://doi.org/10.5194/acp-5-799-2005>
- Riedel, T. P., Bertram, T. H., Crisp, T. A., Williams, E. J., Lerner, B. M., Vlasenko, A., et al. (2012). Nitryl chloride and molecular chlorine in the coastal marine boundary layer. *Environmental Science & Technology*, 46(19), 10,463–10,470. <https://doi.org/10.1021/es204632r>
- Riedel, T. P., Wagner, N. L., Dubé, W. P., Middlebrook, A. M., Young, C. J., Öztürk, F., et al. (2013). Chlorine activation within urban or power plant plumes: Vertically resolved ClNO₂ and Cl₂ measurements from a tall tower in a polluted continental setting. *Journal of Geophysical Research: Atmospheres*, 118, 8702–8715. <https://doi.org/10.1002/jgrd.50637>
- Riedel, T. P., Wolfe, G. M., Danas, K. T., Gilman, J. B., Kuster, W. C., Bon, D. M., et al. (2014). An MCM modeling study of nitryl chloride (ClNO₂) impacts on oxidation, ozone production and nitrogen oxide partitioning in polluted continental outflow. *Atmospheric Chemistry and Physics*, 14(8), 3789–3800. <https://doi.org/10.5194/acp-14-3789-2014>
- Roberts, J. M., Osthoff, H. D., Brown, S. S., & Ravishankara, A. R. (2008). N₂O₅ Oxidizes chloride to Cl₂ in acidic atmospheric aerosol. *Science*, 321(5892), 1059 LP-1059.
- Roberts, J. M., Osthoff, H. D., Brown, S. S., Ravishankara, A. R., Coffman, D., Quinn, P., & Bates, T. (2009). Laboratory studies of products of N₂O₅ uptake on Cl containing substrates. *Geophysical Research Letters*, 36, L20808. <https://doi.org/10.1029/2009GL040448>
- Saiz-Lopez, A., Lamarque, J.-F., Kinnison, D. E., Tilmes, S., Ordóñez, C., Orlando, J. J., et al. (2012). Estimating the climate significance of halogen-driven ozone loss in the tropical marine troposphere. *Atmospheric Chemistry and Physics*, 12, 3939–3949. <https://doi.org/10.5194/acp-12-3939-2012>
- Sander, R. (2015). Compilation of Henry's law constants (version 4.0) for water as solvent. *Atmospheric Chemistry and Physics*. <https://doi.org/10.5194/acp-15-4399-2015>
- Sarwar, G., Simon, H., Xing, J., & Mathur, R. (2014). Importance of tropospheric ClNO₂ chemistry across the Northern Hemisphere. *Geophysical Research Letters*, 41, 4050–4058. <https://doi.org/10.1002/2014GL059962>
- Schroder, J. C., Campuzano-Jost, P., Day, D. A., Shah, V., Larson, K., Sommer, J. M., et al. (2018). Sources and secondary production of organic aerosols in the Northeastern US during WINTER. *Journal of Geophysical Research: Atmospheres*, 123, 7771–7796. <https://doi.org/10.1029/2018JD028475>
- Seinfeld, J. H. (1986). *Atmospheric Chemistry and Physics of Air Pollution*. NY: Wiley-Interscience Publication.
- Sherwen, T., Schmidt, J. A., Evans, M. J., Carpenter, L. J., Großmann, K., Eastham, S. D., et al. (2016). Global impacts of tropospheric halogens (Cl, Br, I) on oxidants and composition in GEOS-Chem. *Atmospheric Chemistry and Physics*, 16(18), 12,239–12,271. <https://doi.org/10.5194/acp-16-12239-2016>
- Simpson, W. R., Brown, S. S., Saiz-Lopez, A., Thornton, J. A., & Von Glasow, R. (2015). Tropospheric halogen chemistry: Sources, cycling, and impacts. *Chemical Reviews*, 115(10), 4035–4062. <https://doi.org/10.1021/cr5006638>
- Snider, J. R., & Petters, M. D. (2008). Optical particle counter measurement of marine aerosol hygroscopic growth. *Atmospheric Chemistry and Physics*, 8(7), 1949–1962. <https://doi.org/10.5194/acp-8-1949-2008>
- Sorooshian, A., Brechtel, F. J., Ma, Y., Weber, R. J., Corless, A., Flagan, R. C., & Seinfeld, J. H. (2006). Modeling and characterization of a particle-into-liquid sampler (PILS). *Aerosol Science and Technology*, 40, 396–409.
- Strapp, J. W., Leaitch, W. R., & Liu, P. S. K. (1992). Hydrated and dried aerosol-size-distribution measurements from the Particle Measuring Systems FSSP-300 probe and the deiced PCASP-100X probe. *Journal of Atmospheric and Oceanic Technology*, 9, 548–555.
- Sullivan, A. P., May, A. A., Lee, T., McMeeking, G. R., Kreidenweis, S. M., Akagi, S. K., et al. (2014). Airborne characteristics of smoke marker ratios from prescribed burning. *Atmospheric Chemistry and Physics*, 14, 10,535–10,545.
- Tham, Y. J., Yan, C., Xue, L., Zha, Q., Wang, X., & Wang, T. (2014). Presence of high nitryl chloride in Asian coastal environment and its impact on atmospheric photochemistry. *Chinese Science Bulletin*, 59(4), 356–359. <https://doi.org/10.1007/s11434-013-0063-y>
- Thornton, J. A., Kercher, J. P., Riedel, T. P., Wagner, N. L., Cozic, J., Holloway, J. S., et al. (2010). A large atomic chlorine source inferred from mid-continent reactive nitrogen chemistry. *Nature*, 464(7286), 271–274. <https://doi.org/10.1038/nature08905>
- Vogt, R., Crutzen, P. J., & Sander, R. (1996). A mechanism for halogen release from sea salt aerosol in the remote marine boundary layer. *Nature*, 383(6598), 327–330. <https://doi.org/10.1038/383327a0>
- Wagman, D. D., Evans, W. H., Parker, V. B., Schumm, R. H., Halow, I., Bailey, et al. (1982). The NBS tables of chemical thermodynamic properties: Selected values for inorganic and C₁ and C₂ organic substances in SI units. *Journal of Physical and Chemical Reference Data*, 11(suppl. 2).
- Young, A. H., Keene, W. C., Pszenny, A. A. P., Sander, R., Thornton, J. A., Riedel, T. P., & Maben, J. R. (2013). Phase partitioning of soluble trace gases with size-resolved aerosols in near-surface continental air over northern Colorado, USA, during winter. *Journal of Geophysical Research: Atmospheres*, 118, 9414–9427. <https://doi.org/10.1002/jgrd.50655>
- Zaveri, R. A., Easter, R. C., Fast, J. D., & Peters, L. K. (2008). Model for simulating aerosol interactions and chemistry (MOSAIC). *Journal of Geophysical Research*, 113, D13204. <https://doi.org/10.1029/2007JD008782>